

Lawrence Berkeley National Laboratory

Recent Work

Title

STABILITY OF THE KAPCHINSKIJ-VLADIMIRSKIJ (K-V) DISTRIBUTION IN LONG PERIODIC TRANSPORT SYSTEMS

Permalink

<https://escholarship.org/uc/item/67h581ps>

Author

Hofmann, I.

Publication Date

1982-08-01



Lawrence Berkeley Laboratory

UNIVERSITY OF CALIFORNIA

RECEIVED
LAWRENCE
BERKELEY LABORATORY

Accelerator & Fusion Research Division

100 10 1982

LIBRARY AND
DOCUMENTS SECTION

To be published in Particle Accelerators

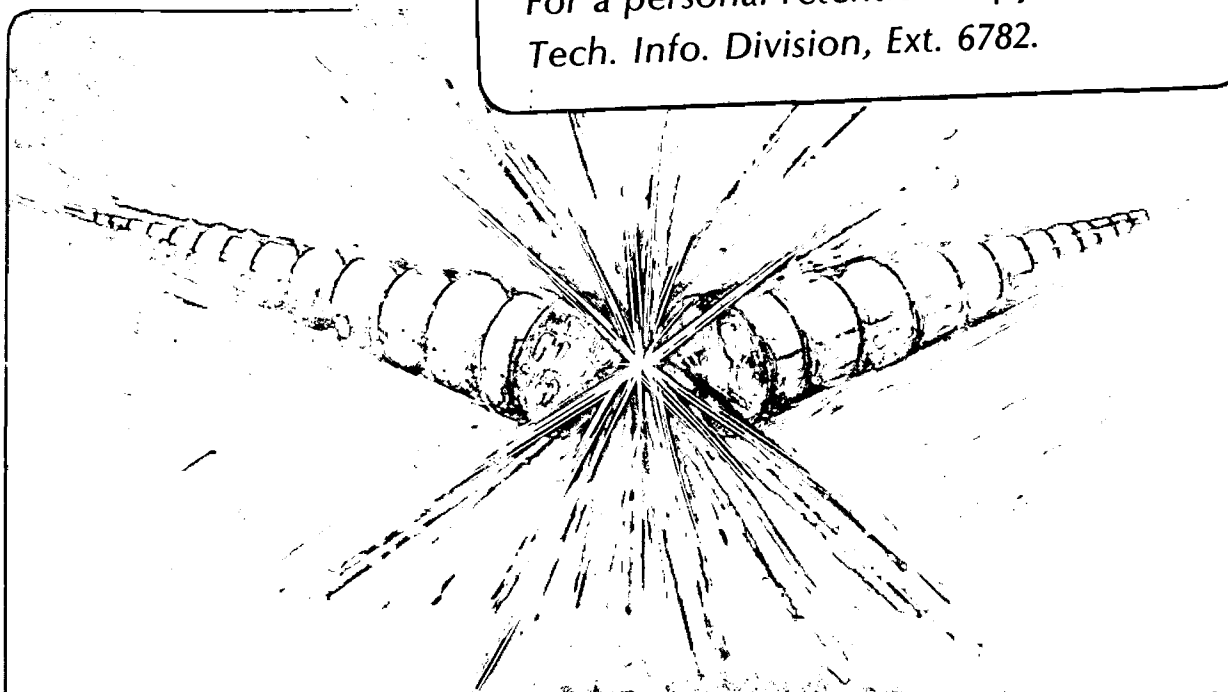
STABILITY OF THE KAPCHINSKIJ-VLADIMIRSKIJ (K-V)
DISTRIBUTION IN LONG PERIODIC TRANSPORT SYSTEMS

I. Hofmann, L.J. Laslett, L. Smith and I. Haber

August 1982

TWO-WEEK LOAN COPY

*This is a Library Circulating Copy
which may be borrowed for two weeks.
For a personal retention copy, call
Tech. Info. Division, Ext. 6782.*



LBL-14922
c.2

DISCLAIMER

This document was prepared as an account of work sponsored by the United States Government. While this document is believed to contain correct information, neither the United States Government nor any agency thereof, nor the Regents of the University of California, nor any of their employees, makes any warranty, express or implied, or assumes any legal responsibility for the accuracy, completeness, or usefulness of any information, apparatus, product, or process disclosed, or represents that its use would not infringe privately owned rights. Reference herein to any specific commercial product, process, or service by its trade name, trademark, manufacturer, or otherwise, does not necessarily constitute or imply its endorsement, recommendation, or favoring by the United States Government or any agency thereof, or the Regents of the University of California. The views and opinions of authors expressed herein do not necessarily state or reflect those of the United States Government or any agency thereof or the Regents of the University of California.

STABILITY OF THE KAPCHINSKIJ-VLADIMIRSKIJ (K-V) DISTRIBUTION
IN LONG PERIODIC TRANSPORT SYSTEMS*

I. Hofmann**, L.J. Laslett, L. Smith and I. Haber†

Lawrence Berkeley Laboratory
University of California
Berkeley, California 94720

August 1982

* This work was supported by the Assistant Secretary for Defense Programs, Office of Inertial Fusion, Laser Fusion Division, U.S. Department of Energy, under Contract No. DE-AC03-76SF00098.

**Max-Planck Institut für Plasmaphysik, 8046 Garching, West Germany.

† Naval Research Laboratory, Washington, D.C. 20375.

STABILITY OF THE KAPCHINSKIJ-VLADIMIRSKIJ (K-V) DISTRIBUTION
IN LONG PERIODIC TRANSPORT SYSTEMS*

I. Hofmann**, L. J. Laslett, L. Smith and I. Haber†

Lawrence Berkeley Laboratory
University of California
Berkeley, California

Abstract

Transport of intense beams of heavy ions over long distances may be restricted by space-charge induced transverse instabilities. The stability of the microcanonical, or K-V, distribution is analyzed with the help of the Vlasov equation, and reduced to a study of the characteristics of solutions for a set of ordinary differential equations with periodic coefficients. Numerical solutions for various periodic solenoid and quadrupole focusing channels are derived and provide information concerning stable regions of propagation in terms of betatron tune depression. The results are compared with computer simulation examples of beams in solenoid and quadrupole focusing channels to check linear growth rates and establish nonlinear saturation levels of instabilities. Conclusions are drawn for the design of a quadrupole lattice providing stable transport.

* This work was supported by the Assistant Secretary for Defense Programs, Office of Inertial Fusion, Laser Fusion Division, U.S. Department of Energy, under Contract No. DE-AC03-76SF00098.

**Max-Planck-Institut für Plasmaphysik, 8046 Garching, West Germany.

† Naval Research Laboratory, Washington, D.C.

I. INTRODUCTION

The possibility of using high energy heavy ions as the igniting mechanism for inertially confined fusion has necessitated the consideration of transporting currents in the kilo-ampere range for distances of the order of kilometers without significant degradation of beam emittance. In addition to the usual problems of field and alignment tolerances, there arises the question of the stability of beam propagation in a vacuum against fluctuations in self-forces arising from initial deviations from the desired distribution of the beam in the four-dimensional transverse phase space.

The most powerful analytic technique for investigating this problem is a linearization of the Vlasov equation about a known stationary solution, coupled with the appropriate equations for the perturbed electromagnetic fields. If the external focusing force is constant, an infinite variety of stationary solutions can readily be generated, since any function of the Hamiltonian is a solution of the Vlasov equation and the corresponding self electrostatic potential can be obtained by integrating Poisson's equation.⁽¹⁾ It furthermore is possible to show⁽²⁾ that a large class of such stationary solutions is stable against arbitrary fluctuations.

For the more realistic situation of a focusing channel consisting of quadrupoles or discrete solenoids, however, the Hamiltonian function is not a constant of the motion and hence cannot be used directly to provide a stationary solution of the Vlasov equation. To our knowledge, the microcanonical distribution investigated by Kapchinskij and Vladimirskij⁽³⁾ (K-V), for which individual-particle restoring forces are linear functions of the displacement, is the only distribution for which a stationary (i.e., periodic) solution can be constructed. Because of its singular character, it is probably more susceptible to instability than real beams and so we have performed the present investigation concerning its stability characteristics in the hope that the results may serve as a conservative guide to identifying regions in parameter space that might be dangerous.

We proceed by presenting in Sect. II the general framework of the linearized Vlasov analysis. This is followed, in Sect. III, by application to periodic solenoid and to quadrupole focusing systems. Specific results are given (Sect. IV) for several perturbation modes in such systems (with the governing equations becoming increasingly complex for modes of high order) and suggest the particular importance of a "third-order" mode. In Sect. V we compare the linear growth of the third-order mode found in both the analytic theory and in computer simulation. Simulation will also be used to establish the practical significance of the remaining instabilities. The implications of these results are discussed in Sect. VI.

We observe that intensity is frequently related to the ratio ν/ν_0 for beams in a continuous solenoid and to σ/σ_0 in a periodic channel. Here ν denotes the betatron oscillation "frequency" (with time replaced by distance), and σ the phase advance of betatron oscillations per focusing period; ν_0, σ_0 are the corresponding values for zero intensity.

II. GENERAL FORMULATION OF THE LINEARIZED VLASOV ANALYSIS

We use the distance s along the transport channel as the independent variable, and write the total Hamiltonian function as

$$(1) \quad H = \frac{1}{2} (p_x^2 + p_y^2) + \frac{1}{2} [\kappa_x(s)x^2 + \kappa_y(s)y^2] + V(x,y;s),$$

where

$$\kappa_x = K_x - \frac{Q}{a(a+b)}, \quad \kappa_y = K_y - \frac{Q}{b(a+b)},$$

$K_{x,y}$ represent the external force constants

$[\pm B'(s)/[B_0]]$ for quadrupoles, and

$(\frac{1}{2} B/[B_0])^2$ for solenoids in the Larmor frame],

$$Q = \frac{4Nq^2 r_p}{A\beta^2 \gamma^3},$$

q = ion charge, A = ion mass/proton mass,

N = number of ions per unit length,

r_p = classical proton radius, $\frac{e^2}{4\pi\epsilon_0 M_{p,0} c^2}$ (MKSA units),

$a(s)$ and $b(s)$ are respectively the x and y half widths of the matched (periodic) beam envelope [as determined by the K-V envelope equations -- Ref. 3, Eqs. (46) and (47)], and

$$V = \frac{q}{A} \frac{4\pi\epsilon_0 r_p / e}{\beta^2 \gamma^3} \times \text{electrostatic potential function due to perturbations.}$$

The first two terms in Eq. (1) represent the unperturbed Hamiltonian, which is not a constant of the motion for s -dependent focusing, and the terms proportional to Q describe the effect of transverse components of the space-charge force for a K-V distribution.

We now make use of the Courant-Snyder⁽⁴⁾ functions $\beta(s)$ and $\alpha(s)$ for the unperturbed orbits, for which (with dots denoting d/ds)

$$\alpha_{x,y} = -\frac{1}{2} \dot{\beta}_{x,y}, \quad \frac{1}{2} \ddot{\beta}_{x,y} - \frac{1}{4} \dot{\beta}_{x,y}^2 / \beta_{x,y} - 1/\beta_{x,y} = -\beta_{x,y} \kappa_{x,y},$$

and(3,4)

$$\beta_x(s) = a^2(s)/\epsilon, \quad \beta_y(s) = b^2(s)/\epsilon,$$

where $\pi\epsilon$ represents the emittance (assumed to be identical in the two transverse planes). The form of the governing Hamiltonian function can thereby be simplified through introduction of a transformation defined by the generating function

$$(2) \quad F = \frac{x}{\beta_x^{1/2}} \left[\bar{p}_x - \frac{\alpha_x}{2} \frac{x}{\beta_x^{1/2}} \right] + \frac{y}{\beta_y^{1/2}} \left[\bar{p}_y - \frac{\alpha_y}{2} \frac{y}{\beta_y^{1/2}} \right],$$

followed by a scaling transformation $\tilde{x} = \bar{x}/\epsilon^{1/2}$, $\tilde{p}_x = \bar{p}_x/\epsilon^{1/2}$, etc.,

so that

$$(3) \quad \tilde{x} = x/(\beta_x \epsilon)^{1/2}, \quad \tilde{p}_x = (\beta_x/\epsilon)^{1/2} [p_x + (\alpha_x/\beta_x)x],$$

and similarly for \tilde{y} , \tilde{p}_y . The new Hamiltonian function then becomes

$$(4) \quad \tilde{H} = \frac{1}{2\beta_x} (\tilde{p}_x^2 + \tilde{x}^2) + \frac{1}{2\beta_y} (\tilde{p}_y^2 + \tilde{y}^2) + \frac{1}{\epsilon} V.$$

In the remainder of this work we shall omit, for brevity, the tilde that distinguishes these new (dimensionless) phase-space variables. In terms of these variables the unperturbed orbits can now be written as pseudo-harmonic oscillations

$$(5) \quad \left. \begin{aligned} x(s') &= x(s) \cos [\psi_x(s') - \psi_x(s)] + p_x(s) \sin [\psi_x(s') - \psi_x(s)] \\ p_x(s') &= p_x(s) \cos [\psi_x(s') - \psi_x(s)] - x(s) \sin [\psi_x(s') - \psi_x(s)] \end{aligned} \right\}$$

with $\psi_x(s) = \int^s dz/\beta_x(z)$, and similarly for $y(s')$ and $p_y(s')$.

From Eqs. (5) it is evident that $x^2 + p_x^2$ and $y^2 + p_y^2$ are individually constants of the unperturbed motion. The unperturbed K-V distribution function, moreover, may now be written as

$$(6) \quad f_0 = \frac{N}{\pi^2} \delta(x^2 + p_x^2 + y^2 + p_y^2 - 1),$$

with δ denoting the Dirac delta function.

With the introduction of a perturbing distribution function f_1 , the linearized Vlasov equation provides the total derivative along the unperturbed trajectories in phase space,

$$(7) \quad \begin{aligned} \frac{Df_1}{Ds} &\equiv \left\{ \frac{\partial}{\partial s} + \frac{1}{\beta_x} \left[p_x \frac{\partial}{\partial x} - x \frac{\partial}{\partial p_x} \right] + \frac{1}{\beta_y} \left[p_y \frac{\partial}{\partial y} - y \frac{\partial}{\partial p_y} \right] \right\} f_1 \\ &= \frac{2N}{\pi^2 \epsilon} \left[p_x \frac{\partial V}{\partial x} + p_y \frac{\partial V}{\partial y} \right] \cdot \delta' \left(x^2 + p_x^2 + y^2 + p_y^2 - 1 \right), \end{aligned}$$

wherein δ' denotes the derivative of the delta function with respect to its argument. Equation (7) can be solved by integrating over the unperturbed trajectories.

Introducing $\psi'_{x,y} \equiv \psi_{x,y}(s')$ as ancillary variables, Eq. (7) thus leads to

$$(8) \quad f_1 = \frac{2N}{\pi^2 \epsilon} \left[\int^s ds' \left(\frac{\partial}{\partial \psi'_x} + \frac{\partial}{\partial \psi'_y} \right) V(x', y'; s') \right] \delta' \left(x^2 + p_x^2 + y^2 + p_y^2 - 1 \right)$$

and (when we neglect the longitudinal field component) Poisson's equation becomes, in terms of our scaled variables and the associated distribution function,

$$(9) \quad \nabla^2 V \equiv \frac{1}{a^2} \frac{\partial^2 V}{\partial x^2} + \frac{1}{b^2} \frac{\partial^2 V}{\partial y^2} = -\frac{Q}{\pi \epsilon ab} \int_0^s ds' \left(\frac{\partial}{\partial \psi'_x} + \frac{\partial}{\partial \psi'_y} \right) \int_0^\infty d(p^2) \delta'(p^2 - (1 - x^2 - y^2)) \int_0^{2\pi} d\theta V(x', y'; s'),$$

subject to the boundary condition that the external fields vanish at infinity. (5)

By noting that

$$(10) \quad \int_0^\infty dz g(z) \delta'(z - z_0) = -\left. \frac{dg}{dz} \right|_{z=z_0} - g(0) \delta(z_0),$$

we see that Poisson's equation, as expressed by Eq. (9), leads to (i)

$$(11) \quad \frac{1}{a^2} \frac{\partial^2 V}{\partial x^2} + \frac{1}{b^2} \frac{\partial^2 V}{\partial y^2} = \frac{Q}{\pi \epsilon ab} \int_0^s ds' \left(\frac{\partial}{\partial \psi'_x} + \frac{\partial}{\partial \psi'_y} \right) \left[\left. \frac{d}{d(p^2)} \int_0^{2\pi} d\theta V(x', y'; s') \right] \right|_{p^2 = 1 - x^2 - y^2}$$

in the interior of the beam, and (ii) to a relation that reflects the presence of an effective surface charge (that describes the effect of an infinitesimal perturbation of the beam boundary)

$$(12) \quad \frac{1}{a^2} \frac{\partial^2 V}{\partial x^2} + \frac{1}{b^2} \frac{\partial^2 V}{\partial y^2} = \frac{2Q}{\epsilon ab} \left[\int_0^s ds' \left(\frac{\partial}{\partial \psi'_x} + \frac{\partial}{\partial \psi'_y} \right) V(x', y'; s') \right] \Big|_{p=0} \delta(1 - x^2 - y^2).$$

By introducing elliptic coordinates (ξ, ζ) defined (in terms of our scaled coordinates, for $a > b$) by

$$(13) \quad x = (h/a) \text{Cosh } \xi \cos \zeta \text{ and } y = (h/b) \text{Sinh } \xi \sin \zeta$$

(where $h^2 = a^2 - b^2$, and with $\text{Cosh } \xi = \frac{a}{h}$, $\text{Sinh } \xi = \frac{b}{h}$ at the boundary $x^2 + y^2 = 1$), Eq. (12) may be written

$$(14) \quad \frac{\partial^2 V}{\partial \xi^2} + \frac{\partial^2 V}{\partial \zeta^2} = \frac{2Qh^2}{\epsilon ab} (\text{Cosh}^2 \xi - \cos^2 \zeta) \left[\int_{\rho=0}^s ds' \left(\frac{\partial}{\partial \psi'_x} + \frac{\partial}{\partial \psi'_y} \right) V(x', y'; s') \right] \delta(1 - x^2 - y^2).$$

The discontinuity of the electric field at the beam boundary accordingly becomes

$$(15) \quad \Delta \frac{\partial V}{\partial \xi} = \frac{Q}{\epsilon} \int_{\rho=0}^s ds' \left(\frac{\partial}{\partial \psi'_x} + \frac{\partial}{\partial \psi'_y} \right) V \left(\cos \zeta \cos(\psi'_x - \psi_x), \sin \zeta \cos(\psi'_y - \psi_y); s' \right).$$

A consistent solution is obtained if we can find a function $V(x, y; s)$ that satisfies Eqs. (11) and (15), where $\Delta(\partial V / \partial \xi)$ is such as to match the solution interior to the beam to a harmonic $\left(\frac{\partial^2 V}{\partial \xi^2} + \frac{\partial^2 V}{\partial \zeta^2} = 0 \right)$ outwardly decreasing solution external to the beam.

III. APPLICATION TO SOLENOID AND QUADRUPOLE FOCUSING

Finding a closed expression for the solutions of Eqs. (11) and (15) appears hopeless, but a brief inspection of these equations shows that they can be satisfied by potential functions that are finite polynomials in x and y interior to the beam and finite sums of $e^{-n\xi} e^{\pm in\zeta}$ exterior to the beam. Finite polynomials emerge as a result of our choice of a K-V distribution for the stationary beam. The derivative of the delta function in Eq. (7) suggests that the perturbations describe distortions of the hyper-ellipsoid in four-dimensional phase space (cf. final sentence in Sect. III of Ref. 6).

(a) Solenoid Focusing

In the simplest case of continuous s -independent focusing, with $K_x = K_y = K$, $\beta_x = \beta_y = \beta$ and both K and β independent of s , then $\psi_x = \psi_y = s/\beta$ and solutions are of the form $V \propto e^{i\omega s} G(x,y)$. Gluckstern⁽⁶⁾ has concluded that in this case $G(x,y)$ can be expressed by means of hypergeometric functions

$$(16) \quad G = \left(\frac{r}{a}\right)^m \begin{pmatrix} \cos m\phi \\ \sin m\phi \end{pmatrix} {}_2F_1\left(-j, m+j, m+1; \frac{r^2}{a^2}\right)$$

in terms of unscaled polar coordinates, where a is the radius of the unperturbed beam and

$$j = 0, 1, 2, \dots, \quad m = 0, 1, 2, \dots, \quad \text{excluding } j = m = 0.$$

The "order" of the mode (highest power of r appearing in the function G) is $2j + m$. Gluckstern has also indicated⁽⁷⁾ the manner in which this solution may be employed to obtain an algebraic equation whose roots must all be real to insure stability of the matched K-V beam. Stability limits for the modes described here can be conveniently described in terms of the factor v/v_0 by which space-charge forces may be permitted to depress the individual-particle oscillation frequency within the matched beam (Table 1). It is clear that intensities limited to values such that $v/v_0 > 0.3985$ are those for which the $m = 0$ modes may be expected to be

stable, and the results presented in Table 1 suggest that this restriction may also be sufficient to insure stability of the higher order modes for an uninterrupted solenoid transport system.

When the focusing strength of the solenoid is not constant but is periodically s -dependent, the matched beam radius (a) becomes a (periodic) function of s . The function $a(s)$ may be sought computationally in such cases, and the entire investigation of beam stability conducted in a manner analogous to that adopted for quadrupole-focusing systems.

(b) Quadrupole Focusing

For the case of alternating-gradient quadrupole focusing ($K_y(s) = -K_x(s)$) we have not found a general closed form for the potential analogous to that indicated by Eq. (16). The analysis of Sect. II leads, however, to a procedure that can be followed to determine the stability characteristics of individual perturbation modes. As will be shown, moreover, the eigenvalues that characterize the stability or instability of a mode can be determined by reference solely to terms of the highest power in x and y and of highest harmonic order in ξ in Eqs. (11) and (15).

(i) Example:

To illustrate this procedure we first consider a simple example that will be seen to correspond to a coherent oscillation of the beam as-a-whole. In this example the internal potential is assumed to be, in terms of the scaled coordinate x , $V_j = A(s)x$.

TABLE 1

Threshold Values of v/v_0

a) For Modes of Even Order

Order, $2j + m$	m	0	2	4
2		Stable	Stable	- - - -
4		0.2425	Stable	Stable
6		0.3859	0.1741	Stable
8		0.3985	0.2582	0.1384
10		0.3972	0.2314 ⁻	0.1396
12		0.3921	0.1885	0.2940
14		0.3861	0.1971 ⁺	0.3205 ⁻
16		0.3798	0.1898 ⁻	0.3263
18		0.3728 ⁻	0.2062 ⁻	
20		0.3680	0.2305	

b) For Modes of Odd Order

Order, $2j + m$	m	1	3	5
1		Stable	- - - -	- - - -
3		Stable	Stable	- - - -
5		Stable	Stable	Stable
7		0.2874	0.2184	Stable
9		0.3235	0.3124	0.2038
11		0.3373 ⁻	0.3246 ⁺	0.2608
13		0.3425	0.3148	0.2248
15		0.3439 ⁻	0.2968	0.2072
17		0.3432	0.2757	
19		0.3415		

It is seen that Eq. (11) is trivially satisfied by this potential function, since $\nabla^2 V = 0$ and

$$\begin{aligned} & \frac{d}{d(p^2)} \int_0^{2\pi} d\theta x' \\ &= \frac{d}{d(p^2)} \int_0^{2\pi} d\theta \left[x \cos(\psi'_x - \psi_x) + p \cos \theta \sin(\psi'_x - \psi_x) \right] = 0. \end{aligned}$$

To treat the boundary equation (15) we employ the elliptic coordinates introduced earlier, writing V_i as $V_i = A(s)(\text{Cosh } \xi / \text{Cosh } \xi_0) \cos \zeta$ and taking the exterior potential to be $V_o = A(s)e^{-(\xi - \xi_0)} \cos \zeta$, where ξ_0 is such that $\text{Cosh } \xi_0 = a/h$. By employing these forms,

$\Delta \frac{\partial V}{\partial \xi} = -A(s) \frac{a+b}{a} \cos \zeta$ and Eq. (15) leads to the integral equation

$$(17) \quad \frac{a+b}{a} A(s) = \frac{Q}{\epsilon} \int_s^S ds' A(s') \sin(\psi'_x - \psi_x).$$

Then by differentiating twice the integral ($I(s)$) that appears in Eq. (17), one finds that it satisfies the differential equation

$$\begin{aligned} (18) \quad \frac{d^2 I}{d\psi_x^2} &= - \left[I + \beta_x A(s) \right] \\ &= - \left[1 + \frac{Q}{\epsilon} \frac{\beta_x a}{a+b} \right] I \\ &= - \left[1 + \frac{\beta_x^2 Q}{a(a+b)} \right] I. \end{aligned}$$

With the quantities a , b , β_x , and ψ_x determinable (e.g., numerically) as periodic functions of s , numerical integrations of Eq. (18) through one period of the transport channel will provide the elements of the matrix that advances the vector I , dI/ds through this interval. The eigenvalues of this matrix provide the frequency of the perturbation

mode, and none may have an absolute value exceeding unity if this mode is to be stable.

We note that, by use of the previously cited relation connecting the Courant-Snyder parameter β_x (and its derivatives) to the force constant κ_x , the differential equation (18) for \underline{I} in this case may be transformed to

$$(19) \quad \frac{d^2}{ds^2} \left(\sqrt{\beta_x} I \right) + \kappa_x \left(\sqrt{\beta_x} I \right) = 0$$

-- which will be recognized as of the form expected for a simple coherent oscillation. Similarly, adoption of a potential function whose dependence on the scaled coordinates is of the form $V_i = A(s) x^2 + B(s) y^2$ will lead to a pair of coupled second order equations equivalent to those customarily taken to represent a linear perturbation of the envelope equations.

(ii) General Treatment:

More generally, we assume a potential function of the form

$$(20) \quad V_n = \sum_{m=0}^n A_m(s) x^{n-m} y^m + \sum_{m=0}^{n-2} A_m^{(1)}(s) x^{n-m-2} y^m + \dots$$

in the interior. For a given order n , "even" and "odd" modes conveniently may be treated separately on the basis of whether the index m in Eq. (20) is restricted to even or to odd integer values.

For the stability analysis, Eq. (11) provides a set of coupled algebraic equations that relate the functions $A_m(s)$ to integrals of the form

$$(21) \quad I_{j; k, \ell} = \int^s ds' A_j(s') \sin \left[k(\psi'_x - \psi_x) + \ell(\psi'_y - \psi_y) \right]$$

while Eq. (15) provides a second set of such equations, and these equations taken together can be solved (at any s for which $a(s)$, $b(s)$)

are known) to express each individual A_j in terms of the integrals defined by Eq. (21). From Eq. (21), moreover, one finds that

$$(22a) \quad C_{k,\ell}(s) \frac{d}{ds} \left[C_{k,\ell}(s) \frac{dI_{j;k,\ell}}{ds} \right] + I_{j;k,\ell} = - C_{k,\ell}(s) A_j,$$

where

$$(22b) \quad C_{k,\ell} \equiv \left[k/\beta_x + \ell/\beta_y \right]^{-1}.$$

With the A_j obtainable (as just mentioned) in terms of the $I_{j';k,\ell}$, Eqs. (22a) constitute a set of coupled second order differential equations for the latter quantities, and numerical integrations through one period of the structure will provide the elements of the matrix that advances such quantities (and their first derivatives) through one period of the transport channel.

(iii) Computational Procedures:

Computational programs have been devised to perform the computations outlined above, for various modes of order up through $n=6$. Computations of this nature for quite large values of n may not be of practical importance. In a realistic beam with a natural spread of individual particle wavelengths (as may result from a nonlinear space-charge force), it is very unlikely that fine-grained transverse density variations (large n) persist through several periods. Computational results of Sect. IIIa pertaining to focusing in a continuous (s independent) solenoid-focusing system indicate, moreover, that the most stringent stability conditions are those imposed by modes of order less than 6 or 8.

To summarize the procedure followed in examining the stability of any particular perturbation mode, one first specifies the type of periodic lattice one wishes to employ⁽⁹⁾ and a value of beam intensity (e.g., Q -- or the parameter Q' -- cited in Ref. 8). By a convergent iterative procedure one then determines initial conditions (for a , b , and their first derivatives) that lead to periodic (matched) solutions of the envelope equations, and, with this solution obtained, the individual particle tune σ is also obtainable (i.e., from solutions of the equations of motion for

individual particles, or as $\sigma_x = \epsilon \int_0^{2L} ds/a^2$ etc). With this information available, the computations are then repeated to include (for various initial values of the $I_{j;k,\ell}$ and their first derivatives) integration of the differential equations for the integrals $I_{j;k,\ell}$. [Note that integration of these equations requires repeated evaluations of the relations that express the quantities A_j in terms of the $I_{j;k,\ell}$ -- as can be done by use of a matrix-inversion/simultaneous-equation-solver routine.] Such integrations yield the elements of the matrix that advances these integrals (and their first derivatives) through one period of the structure, and the eigenvalues λ (and eigenvectors, if desired) of such a matrix are then determined. The occurrence of any eigenvalue of magnitude greater than unity then is indicative of instability for the perturbation mode under consideration, and the magnitude of such an eigenvalue denotes the factor, per period, by which such a perturbation ultimately (in the linear regime) will be expected to grow.

IV. COMPUTATIONAL RESULTS

Based on the analysis of Sect. III, we have examined computationally the behavior of several types of modes -- both for a periodically interrupted solenoid system (Fig. 1a) and for a periodic alternating-gradient quadrupole (FODO) transport channel (Fig. 1b), although with greater emphasis on the quadrupole systems.⁽¹⁰⁾ It is convenient and efficient, in all such cases, to employ "scaled variables". Useful parameters for describing a particular situation are the phase advances σ_0 and σ (of individual particle transverse oscillations, per period of the structure, respectively for a zero intensity beam and for a beam of intensity characterized by the parameter Q' ⁽⁸⁾), and (for a given lattice) the "tune depression" factor σ/σ_0 will serve as a useful index of beam intensity.

In addition to the magnitudes of the eigenvalues that characterize the behavior of a perturbation mode, their phase angles, ϕ [defined, with an ambiguity of 360° , as $\tan^{-1} (Im \lambda / Re \lambda)$ and evaluated so that $-180^\circ < \phi \leq 180^\circ$] also are of interest. Thus, with eigenvalues occurring as complex-conjugate and as reciprocal pairs, the development of an instability indicated by an eigenvalue moving away from the unit circle in the complex plane can occur either (i) when eigenvalues become real, or (ii) when at least two pairs are present, as a result of a confluence having occurred at the threshold of instability. In the first of these cases (and if $\phi \neq 0$) the mode frequency becomes locked to the period of the lattice ("inhomogenous" or "structure" resonance).

Results are best presented as regions of instability on a plot of σ vs. Q' , since it has been found that the locations of these regions and the associated growth rates within them depend primarily on σ/σ_0 and are remarkably insensitive to changes of the lattice structure -- particularly for instabilities that arise as a result of a confluence of eigenvalues.

(a) Interrupted-Solenoid Focusing

The solenoid modes we have studied can be classified in terms of indices corresponding to those introduced by Gluckstern.⁽⁶⁾ We present specific results for symmetric interrupted solenoid systems with an occupancy factor of $1/2$ ($n = 1/2$ in Fig. 1a).

(i) Envelope Modes:

$$j = 1, m = 0, \text{ with } V \propto r^2 \text{ and } \delta a_y = \delta a_x;$$

$$j = 0, m = 2, \text{ with } V \propto r^2 \sin 2\phi \text{ and } \delta a_y = -\delta a_x.$$

At zero intensity the true phases of the eigenvalues for these modes are $|\phi| = 2\sigma_0$ and the phase will decrease as the intensity is increased. Accordingly, if $\sigma_0 > 90^\circ$, there thus is the opportunity, with either type of mode, for an instability to develop at an intensity such that $|\phi|$ becomes 180° (an example of a structure resonance). This behavior is illustrated by the curves of $|\phi|$ vs. Q' on Fig. 2 for the case in which $\sigma_0 = 120^\circ$, and by the regions of instability shown on the curves of σ vs. Q' in Fig. 3. From Fig. 3 it is seen that, as expected, the envelope instabilities occur only for $\sigma_0 > 90^\circ$. The instability region for the $\delta a_y = \delta a_x$ mode becomes quite extensive, moreover, when σ_0 is as large as 120° .

(ii) "Fourth Order" and "Sixth Order" Modes:

$$j = 2, m = 0, \text{ with } V \propto r^4 + \text{terms of lower order};$$

$$j = 3, m = 0, \text{ with } V \propto r^6 + \dots$$

As illustrated by Figs. 4 and 5, each of these modes exhibits minor patches of instability -- which may not warrant concern. More significant are the extended regions of instability that are seen to develop for values of σ/σ_0 close to the values of v/v_0 shown in Table 1 for modes of 4th or 6th order respectively (and $m = 0$).

(iii) $R^4 \cos 2\phi$ and $R^4 \cos 4\phi$ Modes:

$$j = 1, m = 2, \text{ with } V \propto r^4 \cos 2\phi + \text{terms of lower order};$$

$$j = 0, m = 4; \text{ with } V \propto r^4 \cos 4\phi.$$

Examination of stability of these modes (choosing $\sigma_0 = 120^\circ$, 90° , and 60°) indicates the occurrence only of short patches of instability -- as are expected to become possible (for $\sigma_0 > 45^\circ$) when eigenvalues with initial phase angles of $4\sigma_0$ (or $2\sigma_0$) cross the real axis as the intensity is increased, but that have been seen also to arise as a result of a confluence. No extensive regions of instability are found, however, and one notes that no instability of these modes is expected in a continuous solenoid (see Table 1).

(b) FODO Quadrupole Focusing

We have investigated the behavior of several modes, for different values of the occupancy factor n , in the symmetrical lattice of Fig. 1b. It is noticeable that for quadrupole focusing the instabilities of a given order become more numerous than found for the $m = 0$ solenoid modes. This occurs because, for example, the solenoid modes ($j = 3, m = 0$), ($j = 2, m = 2$), ($j = 1, m = 4$), and ($j = 0, m = 6$) are all contained in the sixth order quadrupole case, but extended regions of instability appear in close analogy to the solenoid case. It appears, however, that the onset of regions of pronounced instability can be associated either with a definite value of eigenvector phase Φ (as in the case of the envelope instability) or with a value of σ/σ_0 that depends only slightly on the occupancy factor (n) of the lattice and on the value of σ_0 , so that specific results will be cited here chiefly for $n = 1/2$ (Fig. 1b). We first present results for modes of even order.

(i) Envelope ("Second-Order Even") Mode:

As was found to be the case for the envelope modes in an interrupted solenoid transport system (Sect. IV, a, i), we find that envelope instabilities in a FODO focusing structure occur only if $\sigma_0 > 90^\circ$. This behavior is illustrated in Fig. 6 for $n = 1/2$, wherefrom it is evident that very extensive regions of instability for this mode develop when σ_0 is substantially greater than 90° .

(ii) Second-Order Odd Mode:

The second order-odd mode will not lead to instabilities in a symmetrical FODO structure if (as is customary) $\sigma_0 < 180^\circ$.

(iii) Fourth-Order Even Mode:

Computations pertaining to the fourth-order even mode (requiring evaluation of the eigenvalues of a 14×14 matrix) indicate the appearance of a substantial number of regions of instability that are of somewhat limited extent (Fig. 7). [In Fig. 7, or in similar graphs, regions of very restricted instability may not always be fully depicted.] For $\sigma_0 < 90^\circ$ [as appears desirable in order to avoid potential envelope instabilities (Sub-sect i)], however, the most substantial instability is that which on Fig. 7 is shown to occur for $Q' \approx 3$. The particular unstable fourth-order mode just mentioned is one in which the eigenvalue λ has assumed a real (positive) value.

This significant extended instability of a fourth-order even mode provides an opportunity to illustrate that the threshold for such a mode is given almost uniquely by σ/σ_0 (Table 2) and that such a threshold value of σ/σ_0 is surprisingly close to a corresponding threshold value of v/v_0 for a continuous solenoid (namely, in this instance, to the value 0.2425 shown in Table 1 for the mode $j = 2, m = 0$, for which the associated phase advance also is zero).

TABLE 2

Instability Thresholds for Extended 4th Order Even Mode

Occupancy Factor n	For $\sigma_0 = 60^\circ$			For $\sigma_0 = 90^\circ$		
	Q'	σ (deg.)	σ/σ_0	Q'	σ (deg.)	σ/σ_0
1	3.055	14.58	0.2430	3.713	22.03	0.2448
1/2	2.572	14.58	0.2430	3.130	22.03	0.2448
1/4	1.925	14.58	0.2430	2.347	22.02	0.2447
1/6	1.598	14.58	0.2430	1.950	22.02	0.2447

(iv) Sixth-Order Even Mode:

As with the fourth-order even mode, the sixth-order even mode exhibits a substantial number of patches of instability and ultimately develops an extended instability when the tune depression is sufficiently great (Fig. 8). As was found for the fourth-order even instability, the onset of this extended instability is given almost uniquely by σ/σ_0 . The threshold value of σ/σ_0 for this mode again is close to a threshold value of v/v_0 for a continuous solenoid -- specifically to the value 0.3859 shown in Table 1 for $j = 3, m = 0$. [It is of interest to note that the maximum threshold value of v/v_0 shown in Table 1 for $m = 0$ modes is not markedly greater than the value cited here, namely the value 0.3985 for $j = 4$, vs. 0.3859 for $j = 3$.]

(v) Third-Order Modes:

The third-order mode shows regions of pronounced instability, that appear to account for simulation results presented in the following Section (Sect. V). Because the quadrupole lenses were taken to be very short in the simulation work, we present our results for cases in which $\eta = 1/6$ or $\eta = 1/10$.

The instabilities are shown in Fig. 9 for a FODO lattice with $\sigma_0 = 90^\circ$ and $\eta = 1/10$. The small region of instability shown on Fig. 9 as originating at $\sigma \approx 57.3^\circ$ and the major instability centered near $\sigma = 45^\circ$ are attributable to eigenvalue phases having been depressed from $\Phi_0 = 3\sigma_0 = 270^\circ$ to become 180° , thus indicating a structure resonance, while the instability that originates for $\sigma \approx 56^\circ$ arises from a confluence of eigenvalues. With $|\lambda|$ seen to become as large as approximately 1.27, it is of interest to examine the possibility of avoiding such a strong instability. The "180-degree" modes may be avoided by use of a lattice for which $\sigma_0 \leq 60^\circ$, and it appears also that no confluent third-order mode then will occur (Fig. 10). We remark in passing that in an interrupted-solenoid focusing system we also have found⁽¹¹⁾ (Fig. 11) unstable 180-degree modes similar to those shown in Fig. 9 for the FODO quadrupole transport system.

(vi) Fifth-Order Mode:

Our computations pertaining to the fifth-order mode did not indicate any substantial instabilities that would account for the simulation results. We find that a quadrupole lattice with $\sigma_0 = 60^\circ$ exhibits only moderate patches of instability for the fifth-order mode until the tune has been markedly depressed to $\sigma \approx 10^\circ$ (Fig. 12).

V. COMPARISON WITH SIMULATION RESULTS

Computer simulation provides a possibility of testing the results obtained from analytic theory (and vice versa). The simulation programs used here are based on the particle-in-cell method; they employ typically $\sim 10^4$ simulation particles and solve Poisson's equation with a fast Poisson solver. Results obtained from different simulation programs developed independently^(12 - 18) have been found to yield essentially the same conclusions (apart from variations due to different statistical sets for the initial distribution).

Simulation not only allows the study of the initial growth of an instability within the validity of the linearized theory (section V (a)); it also provides information on the nonlinear saturation of an instability and its effect on beam quality (for instance the r.m.s. emittance). In section V (b) it will be seen that large linear growth rates do not necessarily induce deterioration of beam quality.

(a) Growth of third-order mode within the linearized theory

The theoretical results obtained for the third-order even mode strongly suggested that this mode could account for the strong instability observed in simulation computations⁽¹⁵⁾ (see also following Section) with a K-V beam whose tune is depressed from $\sigma_0 = 90^\circ$ to $\sigma = 45^\circ$. The expected strong instability is characterized by an eigenvalue that is real, but negative -- a feature indicated by the simulation results, wherein distortions of projected phase-space distributions (and their boundaries) were observed to oscillate with respect to the origin with a period twice that of the structure, while the centroid of the distribution remained essentially undisturbed. A quantitative check of the correspondence between theory and the simulation work accordingly was undertaken in order to establish the validity of each of these approaches. We compared both the relative magnitudes of various moments of the distribution (e.g., $\langle xp_x^2 \rangle_{av.}$, etc.) and the shape of the evolving distortion of projections of the distribution (e.g., for a projection onto the p_y ; y plane). Such comparisons were undertaken both at "full-period" points

(i.e., at the centers of F-quadrupole lenses) and at "half-period" points (centers of D lenses).

In making such a comparison it will be realized that the growing perturbation will be characterized by an arbitrary initial amplitude and phase, so that "x-like" (even) moments ($\langle x^3 \rangle_{av.}$, $\langle xy^2 \rangle_{av.}$, etc.) may be intercompared at full-period points but separately from "y-like" (odd) moments ($\langle y^3 \rangle_{av.}$, $\langle x^2y \rangle_{av.}$, etc.). The growing magnitudes of x-like moments at half-period points in a symmetrical FODO lattice may be compared, however, with the growth of y-like moments at full-period points. All such moments, of course, should grow in magnitude in proportion to $|\lambda|^P$, where P denotes the number of periods traversed by the beam, and should alternate in sign once per period. Simulation data appropriate for evaluation will be restricted to an interval wherein the perturbation has grown sufficiently to dominate statistical noise, but has not become significantly influenced by the onset of (nonlinear) saturation. In practice certain moments are more pronounced than others, and the most pronounced moments accordingly are the most suitable for statistically significant intercomparison.

The theoretical description of a developing instability requires retention of terms beyond the leading term in the expression for the perturbation potential. Since the coefficients that determine the moments depend significantly on the value assigned to σ within the zone of instability, the trajectories of the individual simulation particles were examined to establish a value of $\sigma = 45.7^\circ$ (with an associated theoretical eigenvalue $\lambda = -1.27$, for $\eta = 1/6$). The theoretical values of the coefficients required for the present comparison were then evaluated for these conditions.

(i) Comparison of Moments

The growth and satisfactory intercomparison of x-like moments at full-period points is illustrated by Figs. 13-15, where we have used a value of $\lambda = -1.26$. Curves (a) are based on individual fits of the moments $\langle x^3 \rangle_{av.}$, etc., to curves of the form $Y = S\lambda^{P-18}$, while curves (b) are drawn with the values of S for the respective moments

constrained to be in the theoretically expected ratio. Figures 16-18 similarly indicate the behavior of three y-like moments at full-period points. Analogous plots (not shown) have indicated similar performance for moments evaluated at half-period points, and the values of the respective y-like or x-like moments moreover were found to be correctly related to the values of the corresponding x-like or y-like moments at the full-period points.

(ii) Comparison of Boundary Curves

We investigated the form of significantly distorted boundary curves for a two-dimensional projection of the simulation results arising from a perturbed four-dimensional phase-space distribution. Such simulation results are influenced by statistical fluctuations and may be sensitive to the development of nonlinearities in the dynamics. Comparisons with theory are most effectively made for the (p_x, x) or (p_y, y) projections and we have considered these both at full-period points and at half-period points, since fitting the boundary to the expected theoretical forms for such projections requires adjustment of only one coefficient, namely that giving the initial value of the perturbation. Empirically, the values of this coefficient found from such fits appear to be somewhat better characterized by a growth factor $\lambda = -1.22$ than by $\lambda = -1.26$ (possibly because of an incipient nonlinearity), but the values inferred from data that pertain to periods near $P = 11$ have been found to agree within a few percent with those expected from examination of the moments. A fit to the (p_y, y) projection of the simulation results is shown in Fig. 19 for $P = 16$. Other projections (i.e., y vs. x and p_y vs. p_x) have also shown agreement between the computation and simulation results.

(b) Simulation of beams in long transport systems

The question of (nonlinear) saturation of an unstable mode is beyond the capabilities of a linearized theory and is most convincingly investigated by computer simulation. To this end we are presenting below characteristic examples which shed light on the continuous solenoid K-V instabilities and the "structure" resonances found in periodic focusing.

(i) Solenoid Focusing

The findings of section III (a) have been checked by simulating an initial K-V distribution beam matched to a continuous solenoid focusing system. The intensity is described by the factor v/v_0 , which is assumed to be 0.16 for the example shown in Fig. 20. Azimuthal symmetry has been imposed on the beam, hence all modes evaluated in the first column of Table I ($m = 0$) are expected to be unstable. There is evidence for rapid growth of instabilities of rather low order ($j = 2, 3$). The saturation of these instabilities leads to a different phase space distribution, but evidently to no noticeable increase of phase space volume. The r.m.s. emittance even remains constant within $< 1\%$. This supports the conclusion that the K-V instabilities found for $v/v_0 < 0.39$ (similar in periodic focusing to $\sigma/\sigma_0 < 0.39$) have no effect on beam quality, but only emerge as a result of a non-monotonic distribution function.

(ii) FODO quadrupole focusing

In Fig. 21 we show an initial K-V distribution in a FODO channel with $\sigma_0 = 90^\circ$ and $\sigma = 45.7^\circ$. According to section IV (b) this case is in the center of a third-order "structure" resonance, and projections onto the $x-p_x$ and $y-p_y$ planes clearly show the dominant character of this particular mode. The r.m.s. emittances have grown by a factor of 2.0 in $x-p_x$ and 2.5 in $y-p_y$ after 50 cells (with no further growth).

The third-order "structure" resonance is evidently suppressed in a FODO channel with $\sigma_0 = 60^\circ$. Furthermore simulations of such a 60° system exhibit a qualitative behavior resembling that of a continuous solenoid. Thus even for systems with strongly depressed tune (cases with σ as low as 6° have been simulated) the instabilities result in a rearranged phase-space distribution but saturate before any growth in the r.m.s. emittance is observed. These results suggest that although the system is unstable, in agreement with the analytic predictions, no restriction on allowable tune depression is imposed if r.m.s. emittance is a proper measure of beam quality.^(19,20) This conclusion is illustrated in Fig. 22 with $\sigma = 12.7^\circ$ and an initial "waterbag" distribution (in contrast to the K-V distribution it is assumed that the interior of a hyper-ellipsoid in

four-dimensional phase space is uniformly filled, which produces a more realistic beam). Initial matching has been performed by assuming the same r.m.s. quantities as would apply for an exactly matched K-V distribution. This give rise to 10% r.m.s. emittance growth, due to lack of detailed matching, but no further emittance growth over 100 focusing periods.

Figs. 23 and 24 demonstrate the importance of σ_0 in a more direct way. Fig. 23 gives the ratio of r.m.s. emittance to initial emittance for a K-V distribution initially depressed from $\sigma_0 = 90^\circ$ to $\sigma = 7^\circ$. The emittance is seen to grow rapidly at first and then more slowly for the duration of the run. In Fig. 24 the time is initially depressed from $\sigma_0 = 60^\circ$ to $\sigma = 6^\circ$; there is no detectable change in r.m.s. emittance.

VI. CONCLUSION

The special character of the microcanonical or K-V distribution assumed in the present work may lead to instabilities that would not arise with other, more realistic, distributions. Simulations⁽¹⁶⁾ do, however, suggest that in regions where instability is strong (i.e., lead to substantial growth in r.m.s. emittance) the behavior of non-KV systems does not differ substantially. Some insight into the physical mechanism causing instability for the K-V and other distributions can be obtained from a fluid model⁽¹³⁾ and by invoking the concept of negative energy waves. In particular, the extended regions of instability found for continuous solenoid focusing (which also occur for periodic focusing at the same threshold values in terms of tune depression) can be interpreted as coupling of positive and negative energy oscillations⁽¹⁴⁾ and are a characteristic feature of a distribution function that is a non-monotonic function of the Hamiltonian. These instabilities cause a marked redistribution of density in phase space, but do not lead to a growth in r.m.s. emittance. For quadrupole transport, on the other hand, the strength of the focusing force seems to provide a mechanism which causes emittance growth for $\sigma_0 > 60^\circ$; for smaller values of σ_0 the saturated state is very similar to that reached in the case of continuous focusing. If one disregards the minor patches of instability found analytically as peculiar to the K-V distribution, the results of the linear analysis seem to provide a valid guide for design of periodic transport systems for high intensity beams and are particularly significant for $\sigma_0 > 60^\circ$.

In this spirit it appears prudent not merely to require that $\sigma_0 < 90^\circ$ (in order to avoid significant envelope instabilities), but to impose the restriction $\sigma_0 \leq 60^\circ$ with the object of avoiding a pronounced instability of the third-order mode. If the restriction $\sigma_0 \leq 60^\circ$ is adopted, one may expect that beam intensities will be limited only by potential instabilities of fourth or higher order and that significant instabilities of this nature will not occur for $\sigma/\sigma_0 \gtrsim 0.4$ (see Sect. IV, b, iv, and Table 1) -- e.g., for $\sigma \gtrsim 24^\circ$ if $\sigma_0 = 60^\circ$.

Simulation work indicates that, for $\sigma_0 \leq 60^\circ$, the remaining instabilities saturate at low levels and the r.m.s. emittance is not affected by the rearrangement in phase space. If r.m.s. emittance is an adequate measure of beam quality there is then no limit on allowable tune depression. However, if the transported beam is to be delivered to a small focal spot, a practical limit then would be set ultimately by aberrations in the final focusing system.

The expected transportable intensities or beam power, based on a $60^\circ - 24^\circ$ transport line and the associated maximum beam radii in symmetric FODO quadrupole transport systems are then given by the scaled-variable entries of Table 3. The quantities tabulated in Table 3 are

$$\Theta = K^{1/2} \cdot L, \text{ where } L \text{ is the half-period of the lattice;}$$

$$Q' = \frac{4q^2}{A} \frac{Nr_p}{\beta^2 \gamma^3 \epsilon K^{1/2}}, \text{ where } \pi\epsilon \text{ is the (un-normalized) emittance in either plane (meter radians);}$$

$$u_0 = K^{1/4} \epsilon^{-1/2} a \text{ (maximum scaled beam radius); and}$$

[FM] $\equiv Q' / u_0^{2/3}$ is a "figure of merit" that enters into a formula of the type proposed by Maschke⁽²¹⁾ and analyzed by Reiser⁽²²⁾ for the maximum transportable beam current or power (Eq. 23). (The maximum beam radius becomes less if the intensity is reduced).

$$(23) \quad P = C_5 (A/q)^{4/3} (\gamma-1) (\beta\gamma)^{7/3} \epsilon^{2/3} B_Q^{2/3} \cdot [\text{FM}]$$

$$= C_5 (A/q)^{4/3} (\gamma-1) (\beta\gamma)^{5/3} \epsilon_N^{2/3} B_Q^{2/3} \cdot [\text{FM}],$$

where

$$C_5 = (\pi/\mu_0) c^{-1/3} (M_{p,0} c^2/e)^{4/3} = 3.43 \times 10^{15} \text{ (MKSA units),}$$

$$\epsilon_N = \beta\gamma\epsilon \text{ (meter radians),}$$

and B_Q is the quadrupole pole-tip field (Teslas).

The figure of merit [FM] in Table 3 increases as $\sigma^{-2/3}$ as σ is decreased from 24° , but the required aperture increases also and care must be taken in transporting very high currents that the aperture to length ratio of the quadruples does not become too large. (8,22)

TABLE 3

Scaled-Variable Parameters
for a Tune Depression from $\sigma_0 = 60^\circ$ to $\sigma = 24^\circ$

Occupancy Factor	θ	Q'	u_0	[FM]
.1	1.32	1.66	3.20	.764
2/3	1.42	1.54	3.34	.688
1/2	1.57	1.40	3.54	.601
1/3	1.84	1.19	3.87	.481
1/4	2.09	1.04	4.13	.405
1/5	2.32	.944	4.36	.354
1/6	2.52	.867	4.56	.315
1/8	2.89	.757	4.89	.263
1/10	3.22	.680	5.16	.228
1/20	4.51	.485	6.13	.145

VII. ACKNOWLEDGEMENTS

It is a pleasure to acknowledge our indebtedness to V.O. Brady, J. Bisognano, and S. Chattopadhyay for frequent helpful discussions and assistance during the course of this work.

This work was supported by the Assistant Secretary for Defense Programs, Office of Inertial Fusion, Laser Fusion Division of the U.S. Department of Energy under Contract No. DE-AC03-76SF00098.

VIII. REFERENCES AND NOTES

- 1) See, for example, R.L. Gluckstern, R. Chasman, and K. Crandall, Proc. 1970 Natl. Accelerator Lab. Linear Accelerator Conf. (M.R. Tracy, Ed.), v. 2, p. 823 (FNAL, Batavia, Ill.; 1970).
- 2) R.C. Davidson and N.A. Krall, Phys. Fluids 13, 1543 (1970).
- 3) I.M. Kapchinskij and V.V. Vladimirkij, Proc. 1959 Internat. Conf. High Energy Accelerators, p. 274 (CERN, Geneva, Switzerland; 1959).
- 4) E.D. Courant and H.S. Snyder, Ann. Phys. (NY) 3, 1 (1958).
- 5) This boundary condition is consistent with that used to obtain the space-charge force constant commonly used in the envelope equations.⁽³⁾ We have calculated the image forces produced by an elliptical beam co-axially situated within a circular tube, and find them to be remarkably linear and relatively small -- even if the beam almost touches the wall of the tube. We accordingly conclude that the presence of a vacuum pipe may be neglected for the present purposes.
- 6) R.L. Gluckstern, Proc. 1970 Nat. Accelerator Lab. Linear Accelerator Conf. (M.R. Tracy, Ed.), v. 2, p. 811 (FNAL, Batavia, Ill; 1970).
- 7) Eqn. (19) of Ref. 6, where $v^2/\omega_p^2 = (v/v_0)^2/[1-(v/v_0)^2]$.
For any specified value of v/v_0 the beam intensity is given by⁽⁸⁾
 $Q = 2\epsilon K^{1/2} (v_0/v - v/v_0)$ and the envelope radius by $a^2 = \epsilon K^{-1/2} v/v_0$.
- 8) G.R. Lambertson, L.J. Laslett, and L. Smith, IEEE Trans. Nucl. Sci. NS-24 (No. 3), 933 (1977), wherein $\pi\epsilon$ denotes a normalized emittance (i.e., wherein ϵ is $\beta\gamma$ times our ϵ) and Q represents our $Q' = Q/(\epsilon K^{1/2})$.

- 9) Computations pertaining to a periodic transport channel are conveniently performed in terms of "scaled variables" -- such as introduced in Ref. 8.
- 10) The results summarized in this article have been described in somewhat greater detail in an internal report (HI-FAN-15, Lawrence Berkeley Laboratory; 12 October 1977). With few exceptions, the periodic transport channels we have examined have been symmetrical, in the manner indicated by Figs. 1a - b. In some instances this restriction may result in certain modes remaining stable under conditions such that instability would result if the symmetry were broken -- thus only by such a breaking of the symmetry does the second-order odd mode (or "xy mode") with $\sigma_0 < 180^\circ$ exhibit instability in a FODO quadrupole focusing channel.
- 11) Further discussion and analysis of the third-order instability in a periodic interrupted-solenoid transport system is given in an internal report by Bisognano, Laslett, and Smith (HI-FAN-44, Lawrence Berkeley Laboratory; September, 1978).
- 12) I. Hofmann, IEEE Trans. Nucl. Sci. NS-26 (No. 3), 3083 (1979).
- 13) I. Hofmann, Particle Accelerators 11, 31 (1980).
- 14) P. Lapostolle, IEEE Trans. Nucl. Sci. NS-18 (No. 3), 1101 (1971).
- 15) I. Haber, Proc. Heavy Ion Fusion Workshop (R.C. Arnold, Ed.), ANL-79-41, p. 317 (Argonne Natl. Lab., Argonne, Ill.; 1978).
- 16) I. Haber, IEEE Trans. Nucl. Sci. NS-26 (No. 3), 3090 (1979).
- 17) Samuel Penner and Annija Galejs, IEEE Trans. Nucl. Sci. NS-26 (No. 3), 3086 (1979).

- 18) I. Haber and A.W. Maschke, Proc. Heavy Ion Fusion Workshop (L.W. Smith, Ed.), BNL 50769 (Brookhaven Natl. Lab., Upton, N.Y.; 1977), p. 122.
- 19) I. Bozsik and I. Hofmann, Proc. Conf. Charged Particle Optics, Giessen, Germany, 1980; published in Nucl. Instr. Meth. 187, 305 (1981). I. Haber and A.W. Maschke, Phys. Rev. Letters 42, p. 1479 (1979).
- 20) I. Hofmann, Proc. Conf. Charged Particle Optics, Giessen, Germany, 1980; published in Nucl. Instr. Meth. 187, 281 (1981).
- 21) A.W. Maschke, cited by E.D. Courant in ERDA Summer Study of Heavy Ions for Inertial Fusion (R.O. Bangerter, W.B. Herrmannsfeldt, D.L. Judd, and Lloyd Smith, Eds.), LBL-5543, Appendix 6-2, p. 72 (Lawrence Berkeley Laboratory, Berkeley, Calif. and Lawrence Livermore Laboratory, Livermore, Calif.; 1976).
- 22) M. Reiser, Part. Accelerators 8, p. 167 (1978).

Captions for Figures:

Fig. 1. Assumed periodic transport lattice, (a) with interrupted solenoid elements and (b) with quadrupole lenses. η denotes the fraction of the lattice occupied by lens elements.

Fig. 2. Behavior of envelope modes for an interrupted-solenoid system for which $\eta = 1/2$ and $\sigma_0 = 120^\circ$, with regions of instability indicated by heavy lines on plots of ϕ vs. Q' .

Fig. 3. Behavior of envelope modes for interrupted-solenoid systems for which $\eta = 1/2$ and $\sigma_0 = 120^\circ, 100^\circ, 90^\circ,$ and 60° .

Fig. 4. Behavior of fourth-order mode ($j = 2, m = 0$) for interrupted-solenoid systems for which $\eta = 1/2$ and $\sigma_0 = 120^\circ, 90^\circ,$ and 60° .

Fig. 5. Behavior of sixth-order mode ($j = 3, m = 0$) for interrupted-solenoid systems for which $\eta = 1/2$ and $\sigma_0 = 120^\circ, 90^\circ,$ and 60° .

Fig. 6. Behavior of envelope mode for quadrupole systems with $\eta = 1/2$ and $\sigma_0 = 180^\circ, 150^\circ, 130^\circ, 110^\circ, 100^\circ,$ and 90° .

Fig. 7. Behavior of fourth-order even mode for quadrupole systems with $\eta = 1/2$ and $\sigma_0 = 120^\circ, 90^\circ, 80^\circ,$ and 60° .

Fig. 8. Behavior of sixth-order even mode for quadrupole systems with $\eta = 1/2$ and $\sigma_0 = 80^\circ$ and 60° .

Fig. 9. Behavior of third-order mode for a quadrupole system with $\eta = 1/10$ and $\sigma_0 = 90^\circ$.

Fig. 10. Depression of eigenvalue phase, $|\phi|$, for third-order modes of a quadrupole system with $\eta = 1/6$, and $\sigma_0 = 60^\circ$.

Fig. 11. Behavior of third-order mode for interrupted-solenoid systems for which $\eta = 1/2$ or $\eta = 1/6$ and $\sigma_0 = 90^\circ$.

Fig. 12. Behavior of fifth-order even mode for a quadrupole system with $\eta = 1/6$ and $\sigma_0 = 60^\circ$.

Fig. 13. Growth of the moment $Y = \langle xp_x^2 \rangle_{av.}$ at integer period numbers, from simulation computations. Curve (a) is based on a fit of this individual moment to the form $Y = S\lambda^{p-18}$, while the curve (b) is such that the values of S for this and other moments of the same type are constrained to be in the theoretically expected ratio.

Fig. 14. Growth of the moment $Y = \langle x^2 p_x \rangle_{av.}$

Fig. 15. Growth of the moment $Y = \langle x^5 \rangle_{av.}$

Fig. 16. Growth of the moment $Y = \langle y p_y^2 \rangle_{av}$.

Fig. 17. Growth of the moment $Y = \langle y^2 p_y \rangle_{av}$.

Fig. 18. Growth of the moment $Y = \langle y^5 \rangle_{av}$.

Fig. 19. Boundary of p_y vs. y projection, at period number 16. The crosses denote simulation results and the curve represents the theoretically expected boundary.

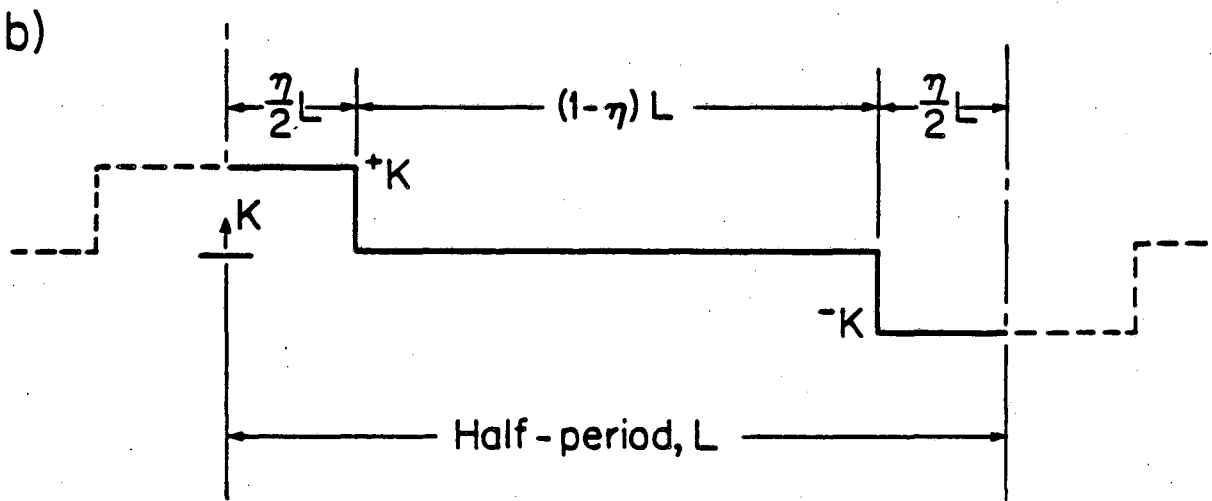
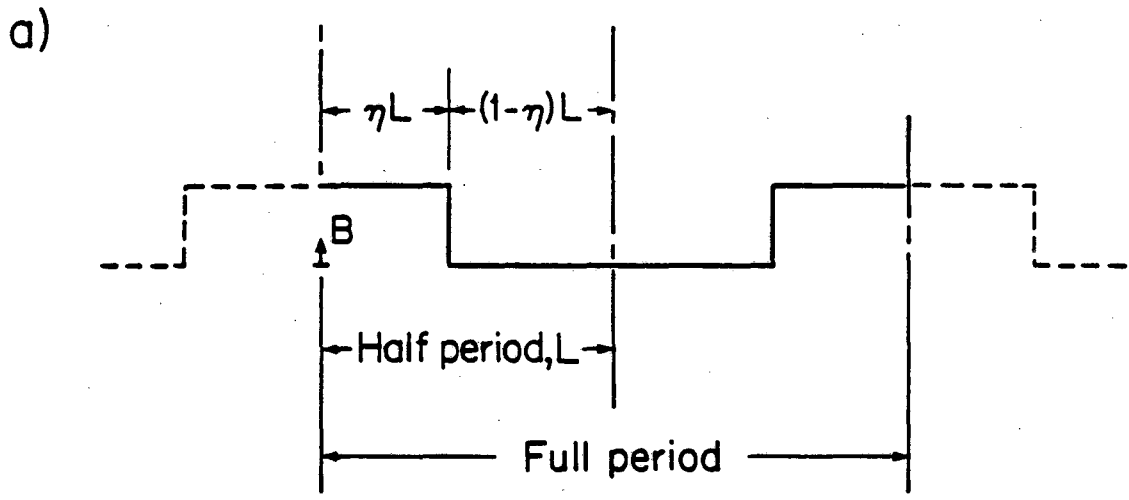
Fig. 20. Phase space projections of initial K-V distribution in a continuous solenoid with $v/v_0 = 0.16$. The beam is assumed azimuthally symmetric with $1.3 \cdot 10^5$ simulation particles. Frames are in time steps of 1/10th of a betatron period.

Fig. 21. Initial K-V distribution in a FODO channel with $\sigma_0 = 90^\circ$, $\sigma = 45.7^\circ$ and $8 \cdot 10^3$ simulation particles. Frames every 5th focusing period.

Fig. 22. Initial "waterbag" distribution (r.m.s. matched) in a FODO channel with $\sigma_0 = 60^\circ$, $\sigma = 12.7^\circ$ and $8 \cdot 10^3$ simulation particles. Frames every 5th focusing period.

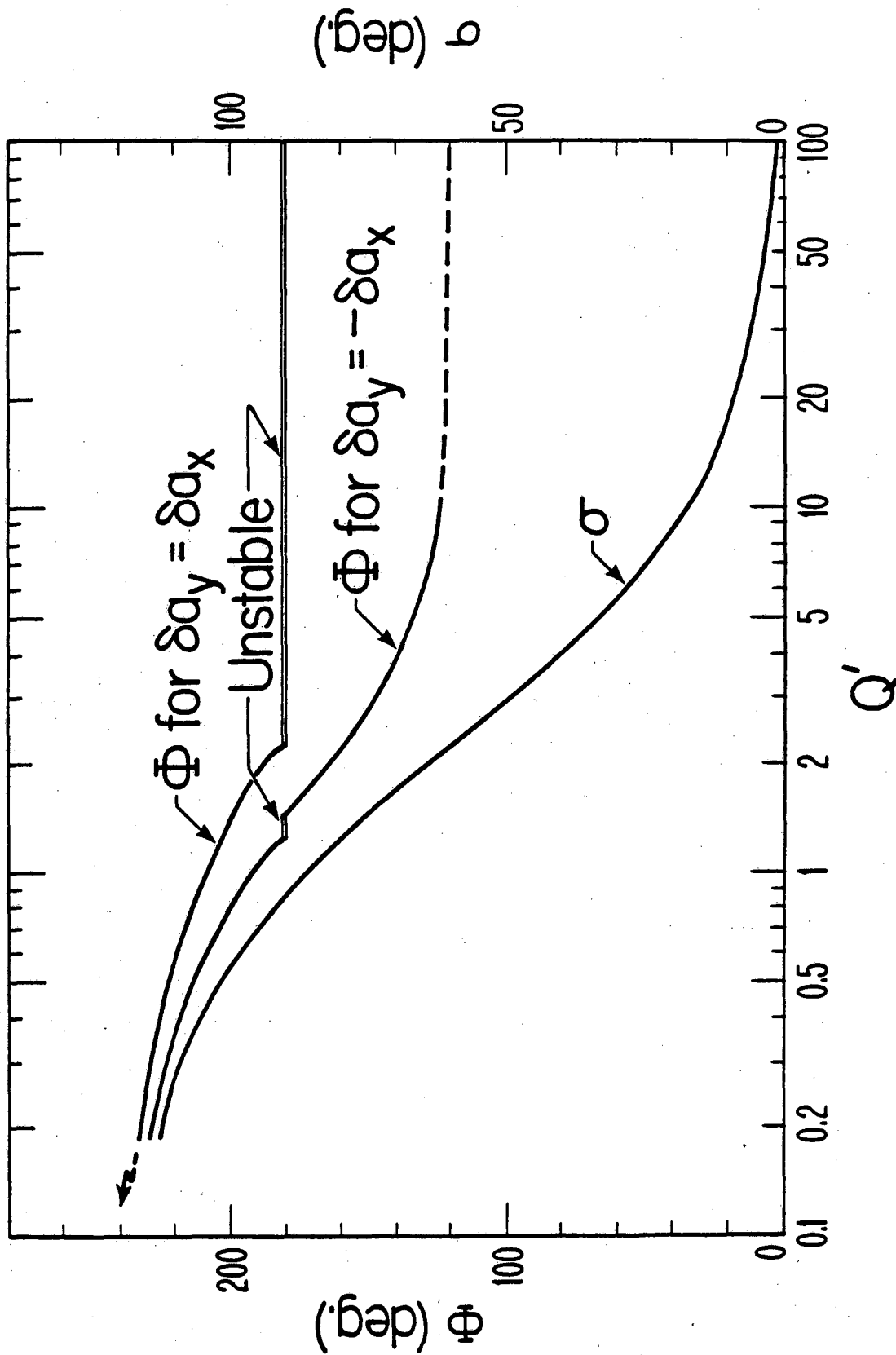
Fig. 23. Ratio of r.m.s. emittance to its initial value for a K-V distribution with $\sigma_0 = 90^\circ$ and $\sigma = 7^\circ$.

Fig. 24. Ratio of r.m.s. emittance to its initial value for a K-V distribution with $\sigma_0 = 60^\circ$ and $\sigma = 6^\circ$.



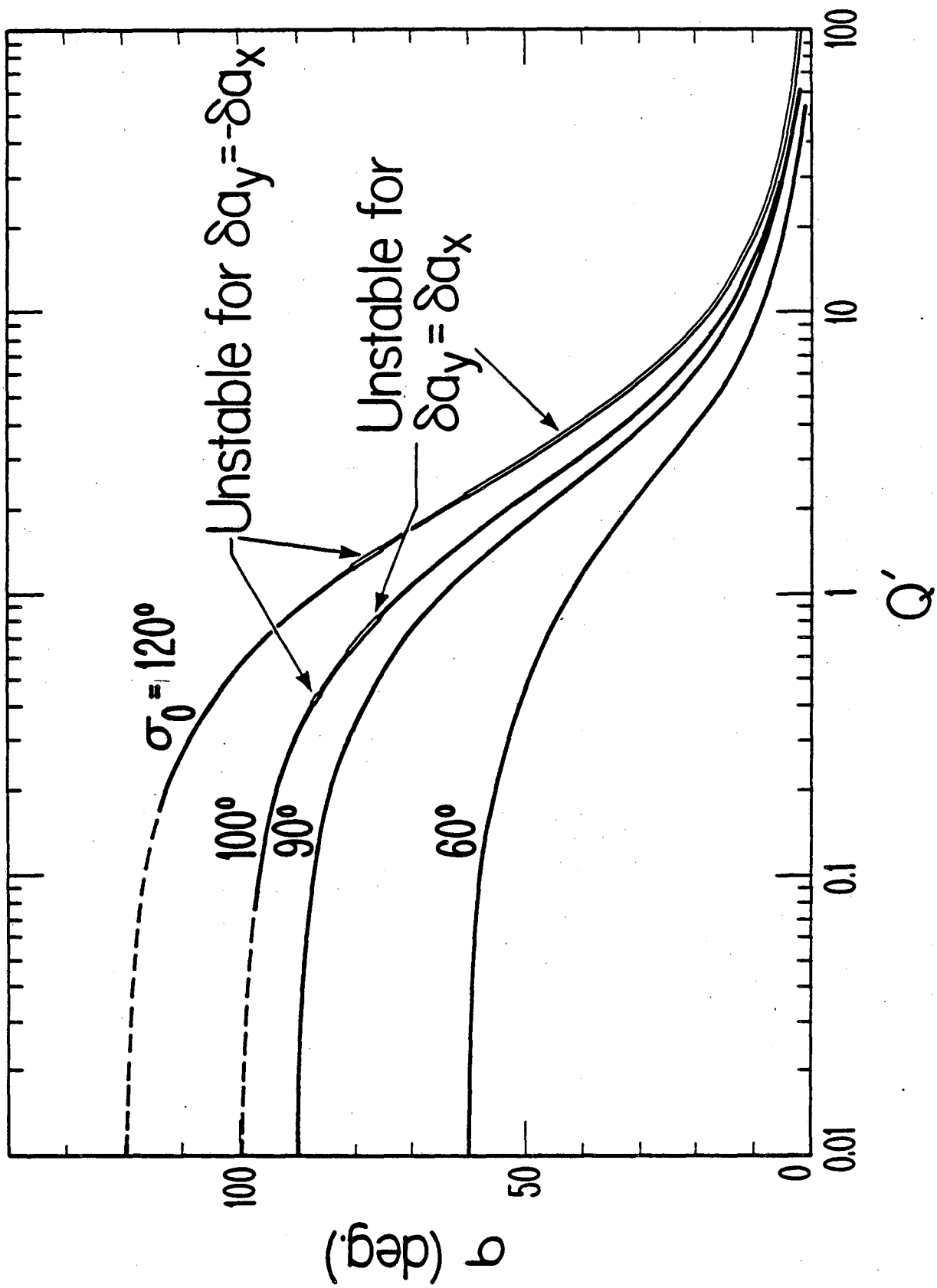
XBL 7910 - 4263

Figure 1



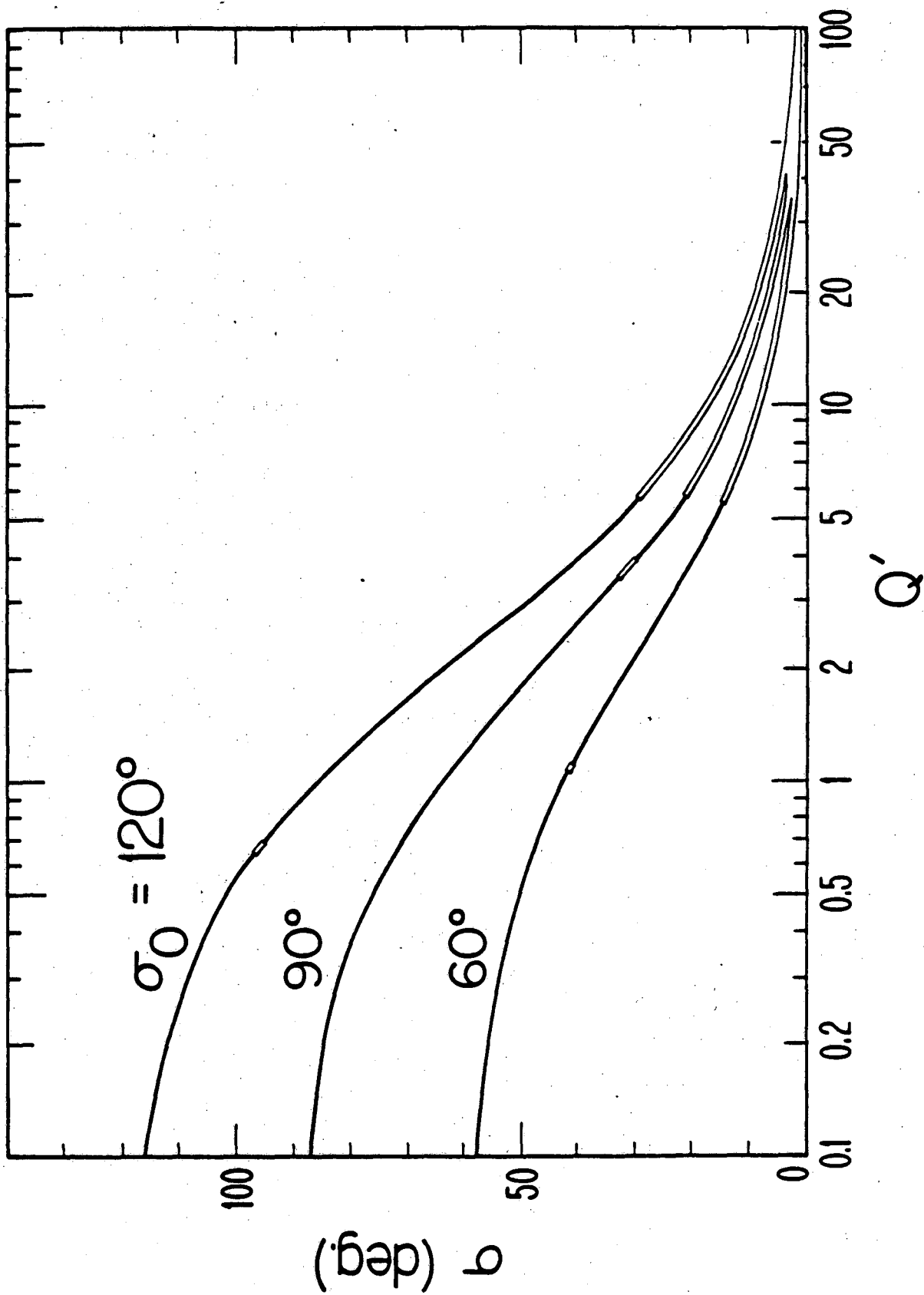
XBL 7910-4264

Figure 2



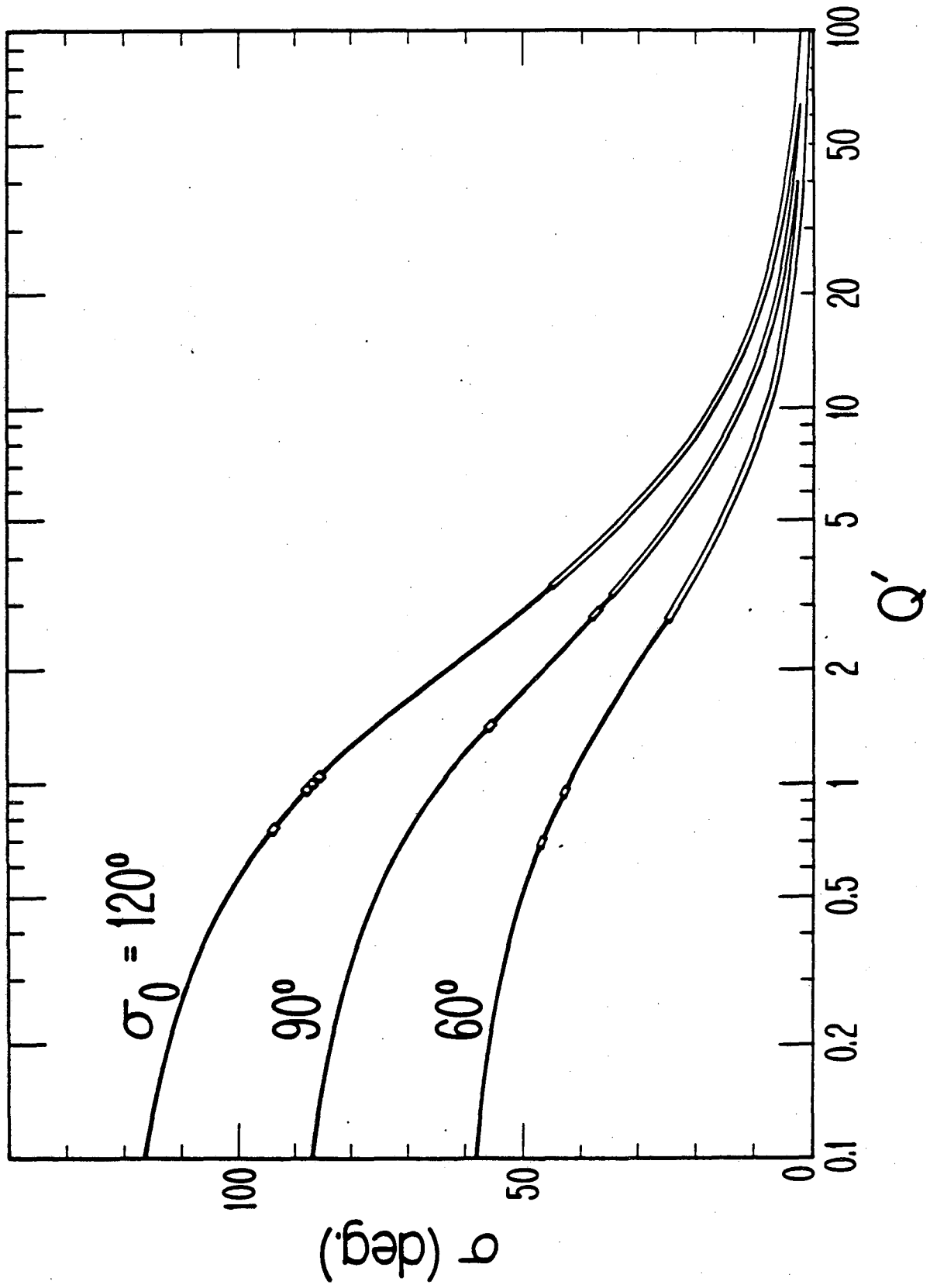
XBL 7910-4279

Figure 3



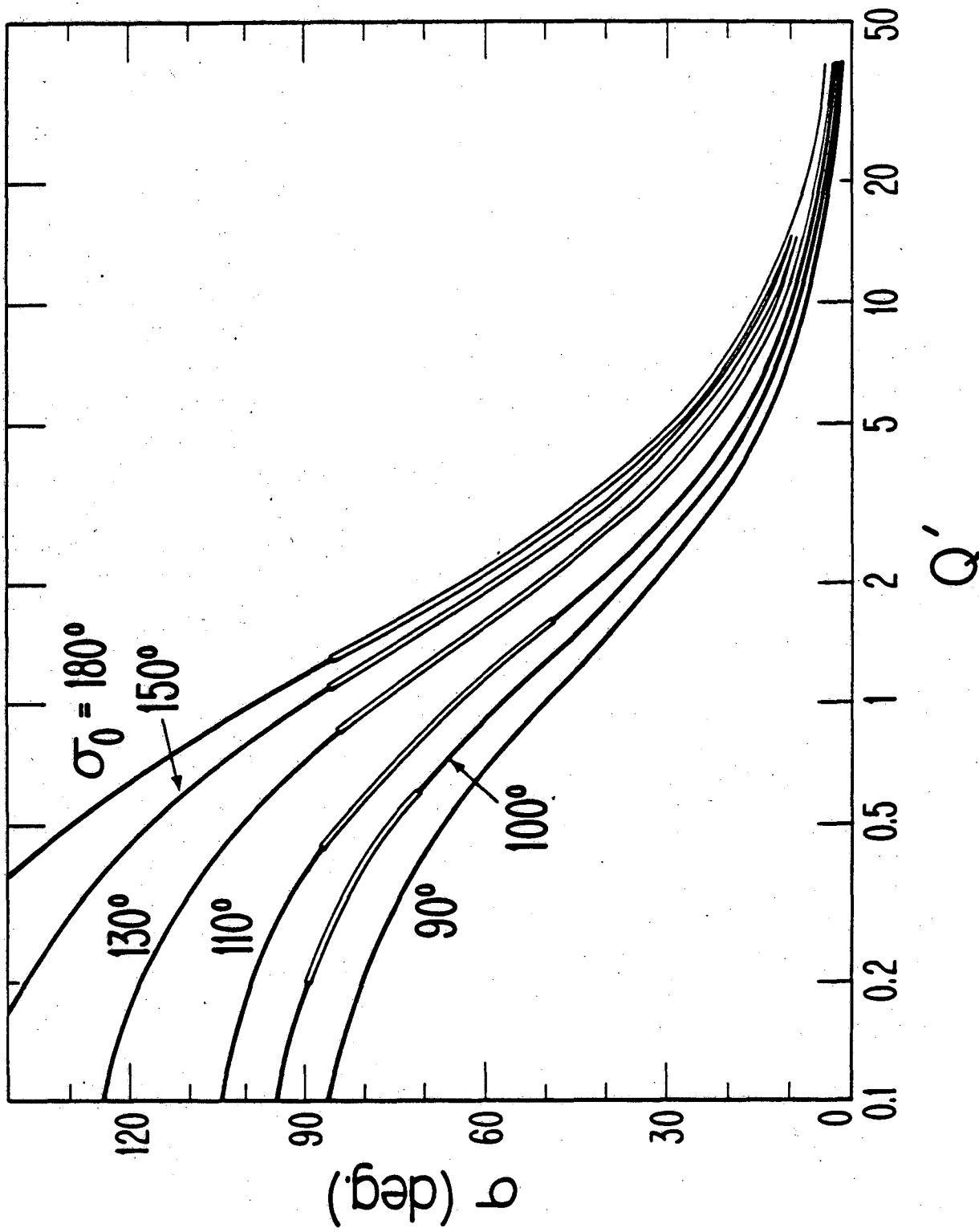
XBL 7910 - 4281

Figure 4



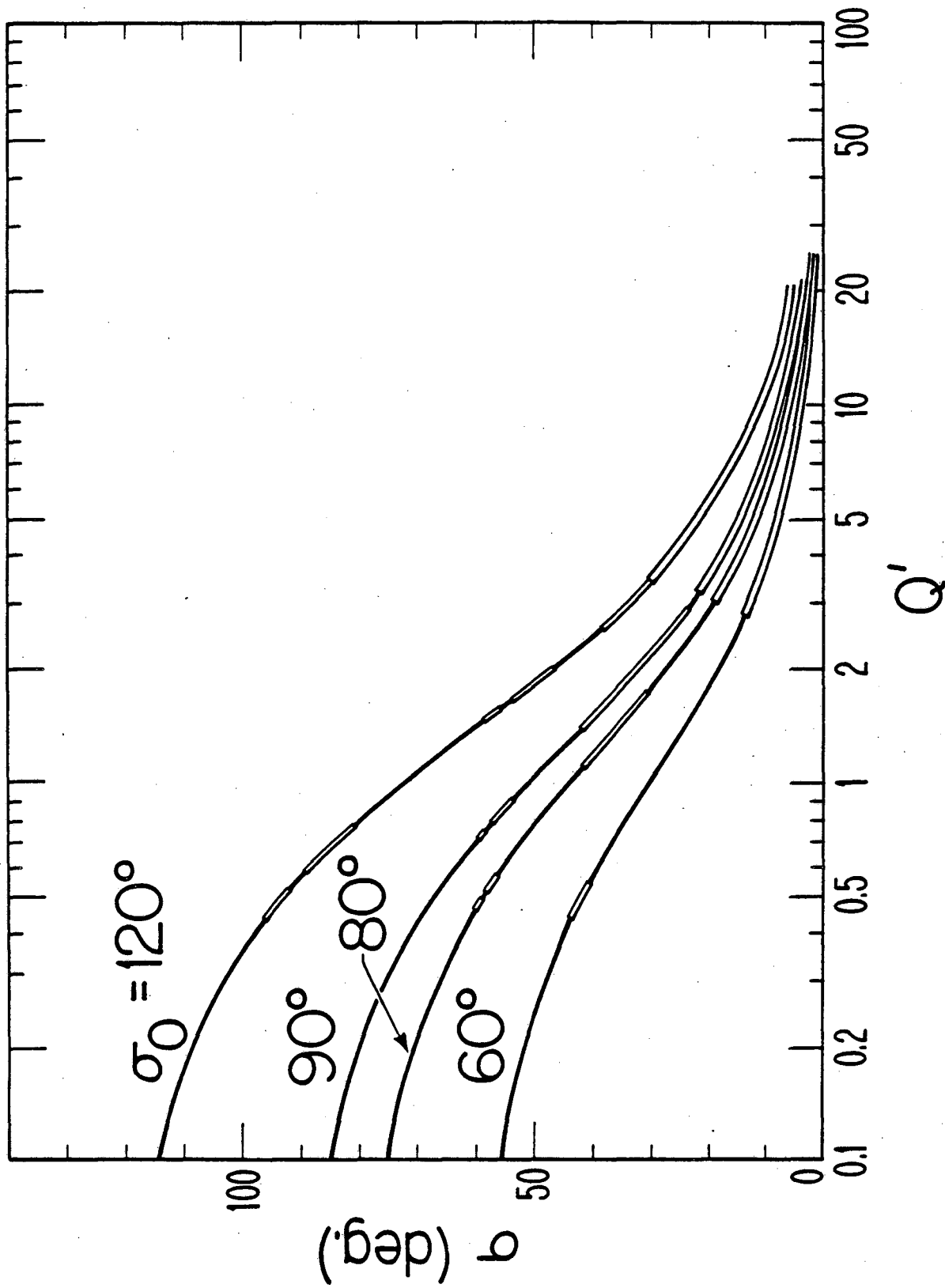
XBL 7910 - 4280

Figure 5



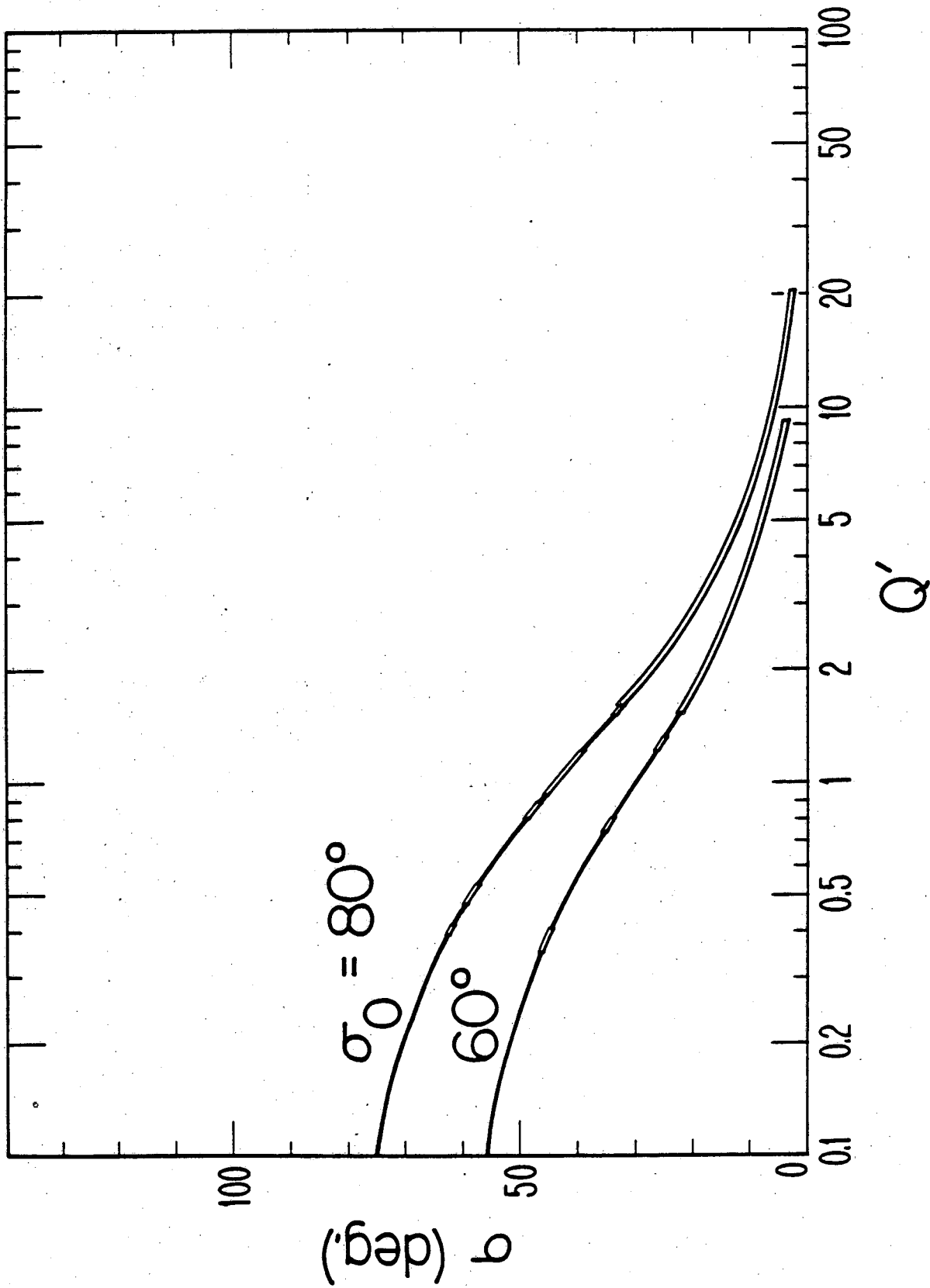
XBL 7910-4278

Figure 6



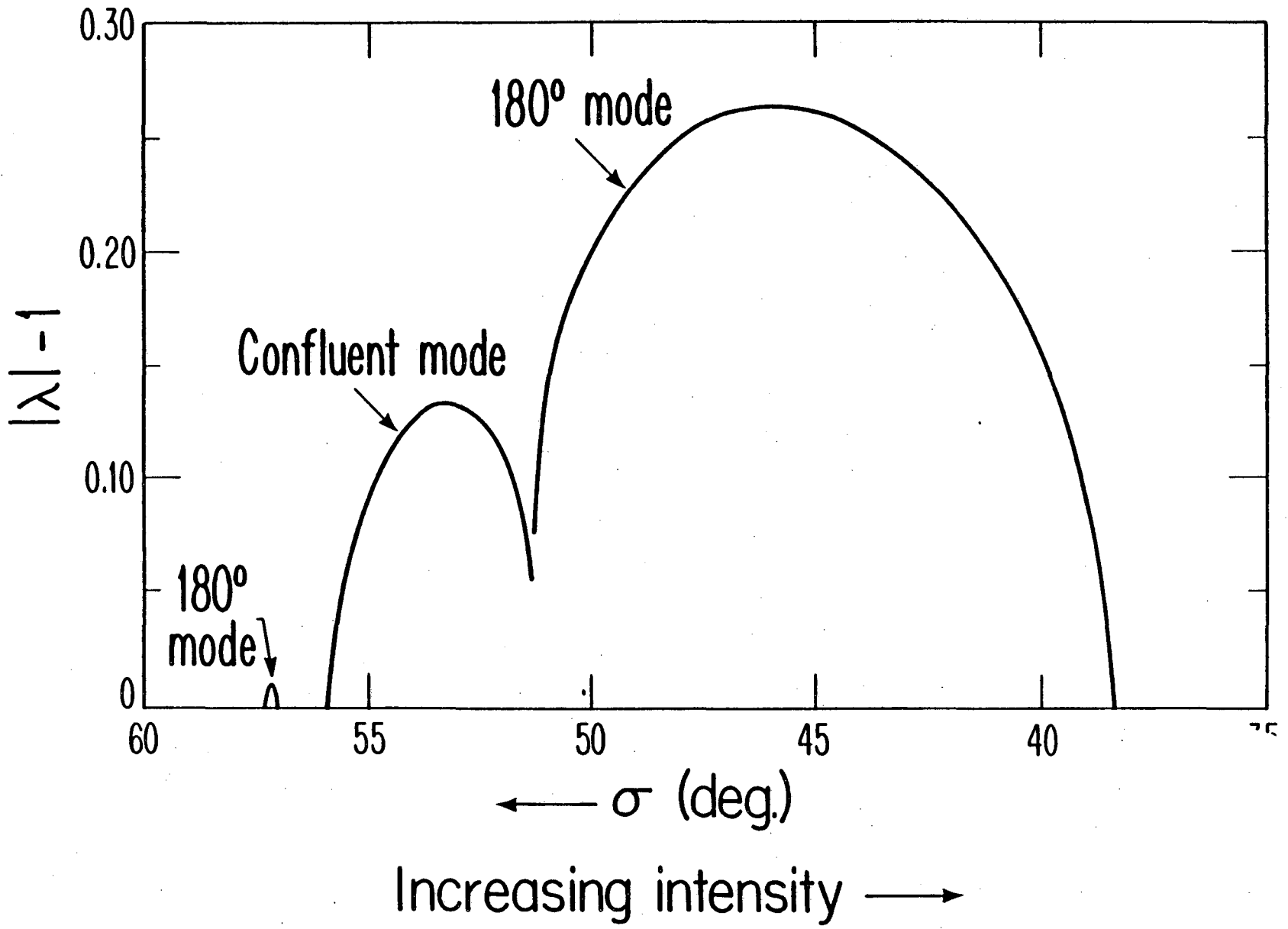
XBL 7910-4266

Figure 7



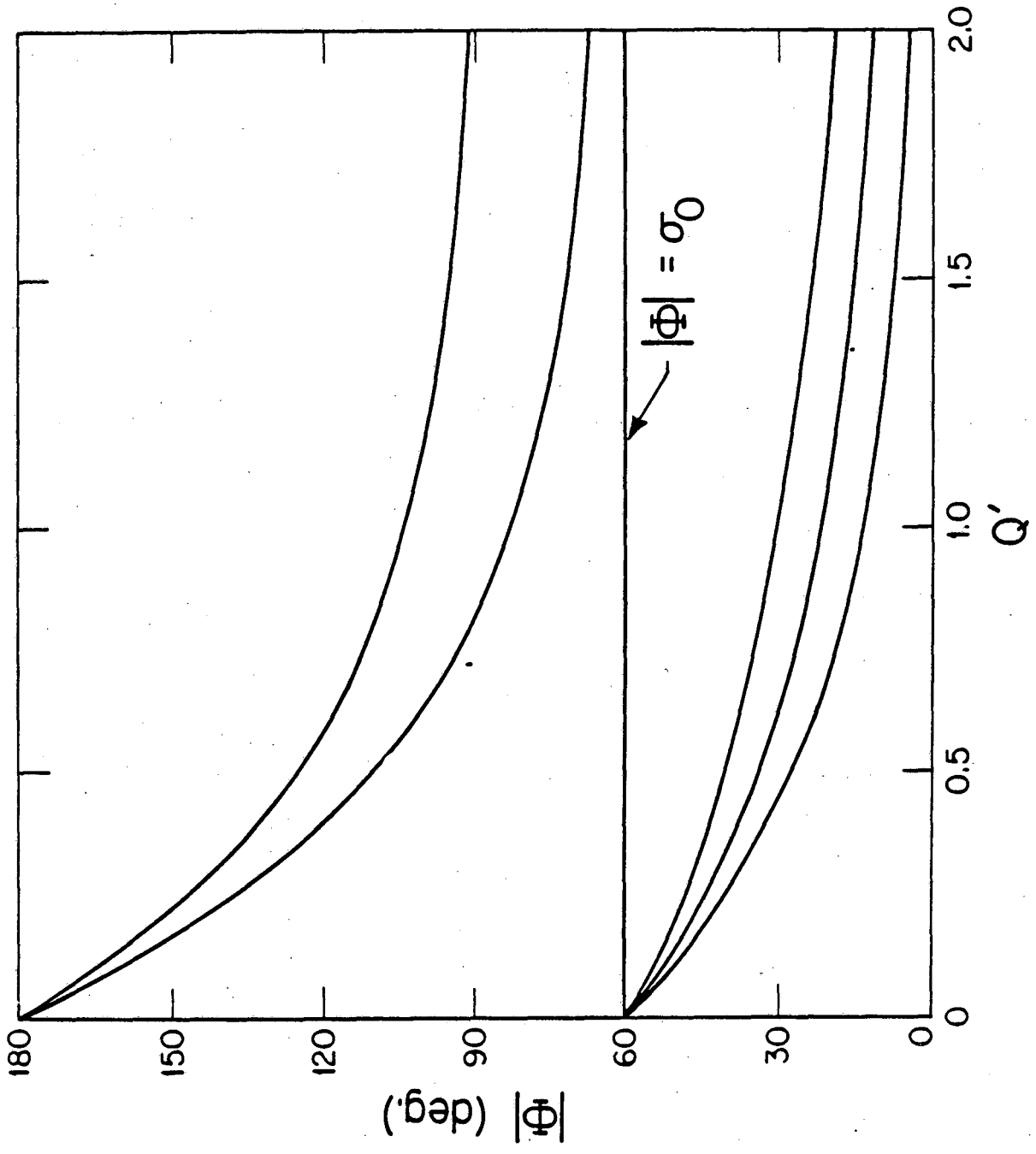
XBL 7910 - 4265

Figure 8



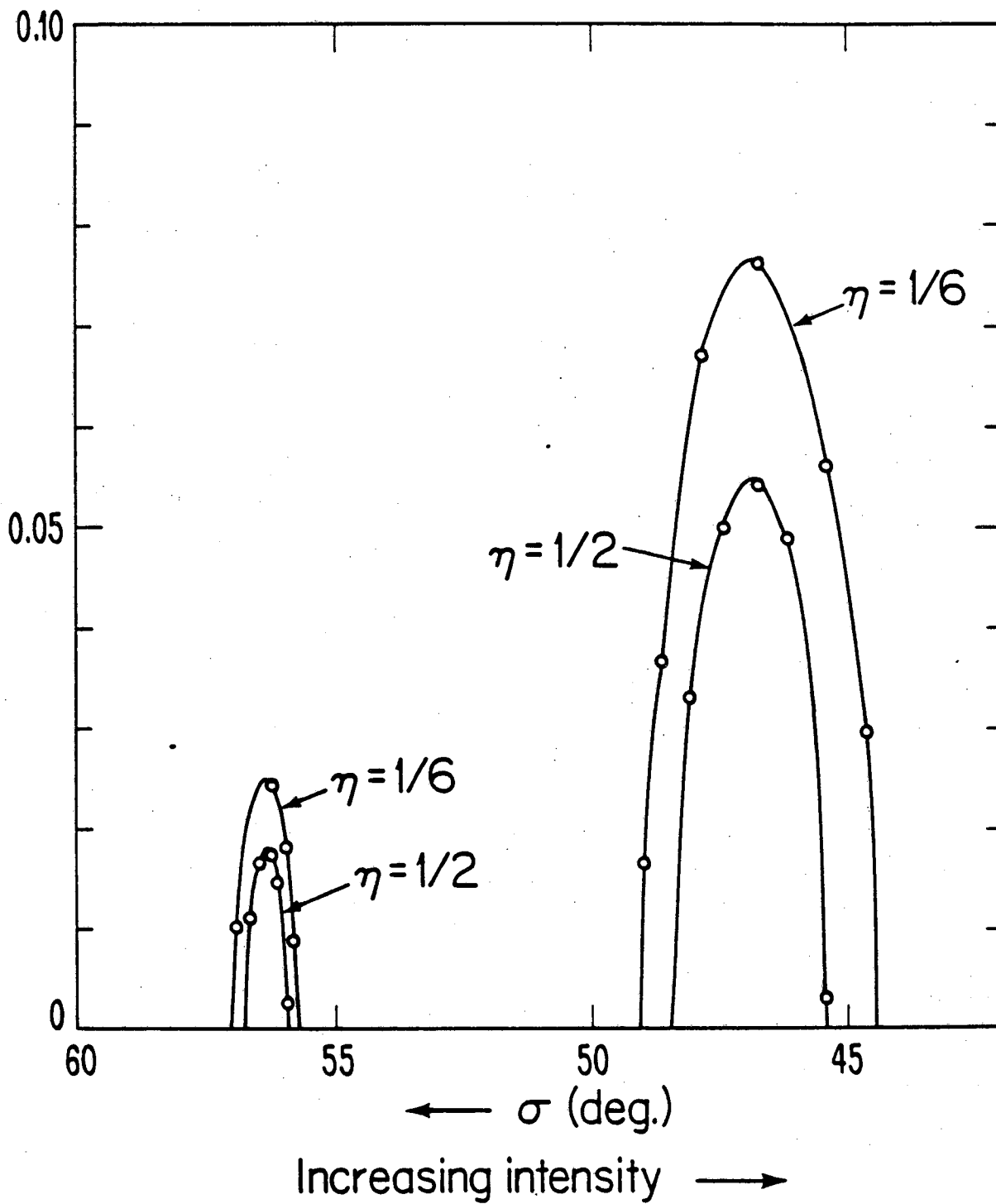
XBL 7910-4268

Figure 9



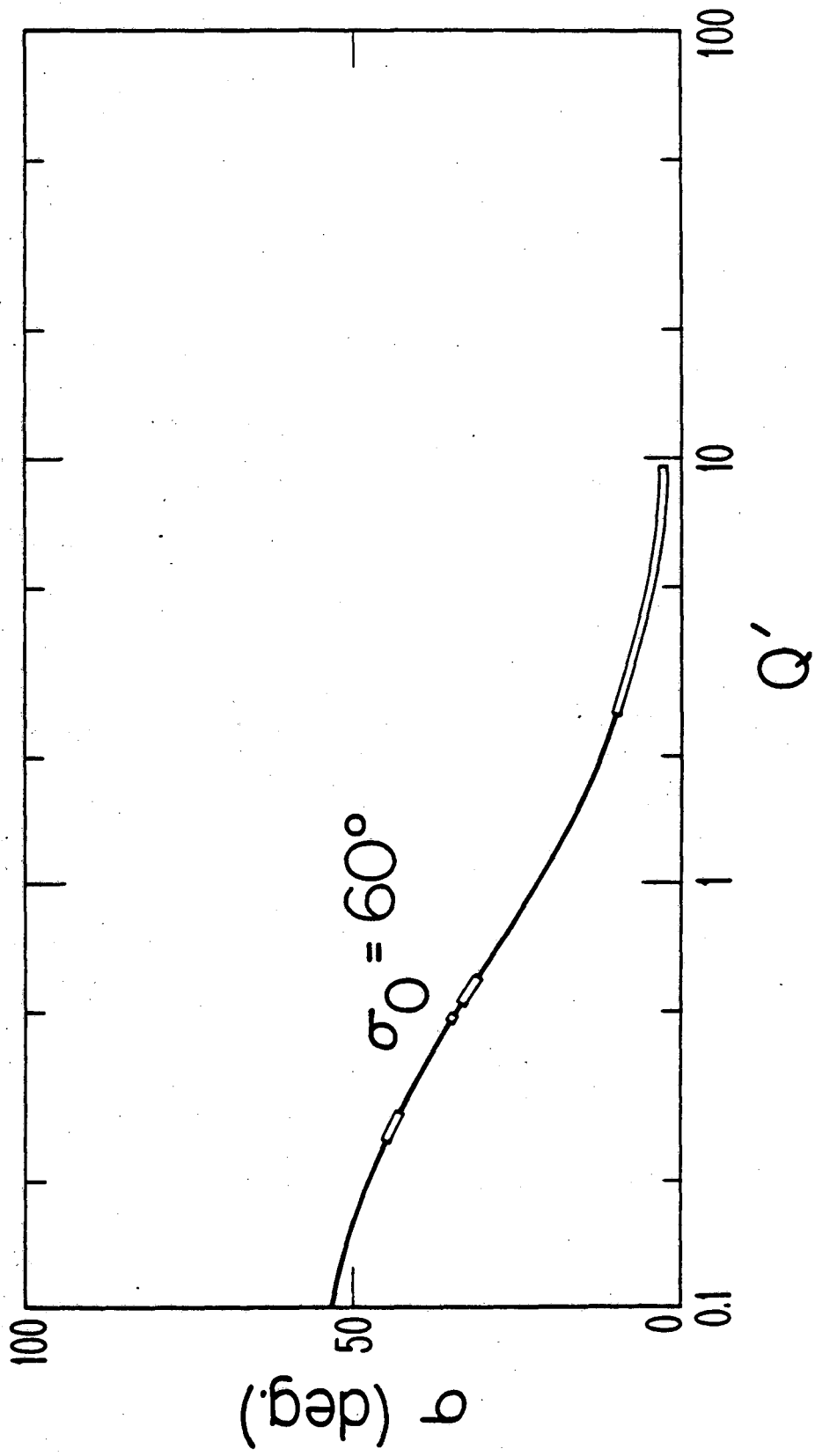
XBL 7910 - 4270

Figure 10



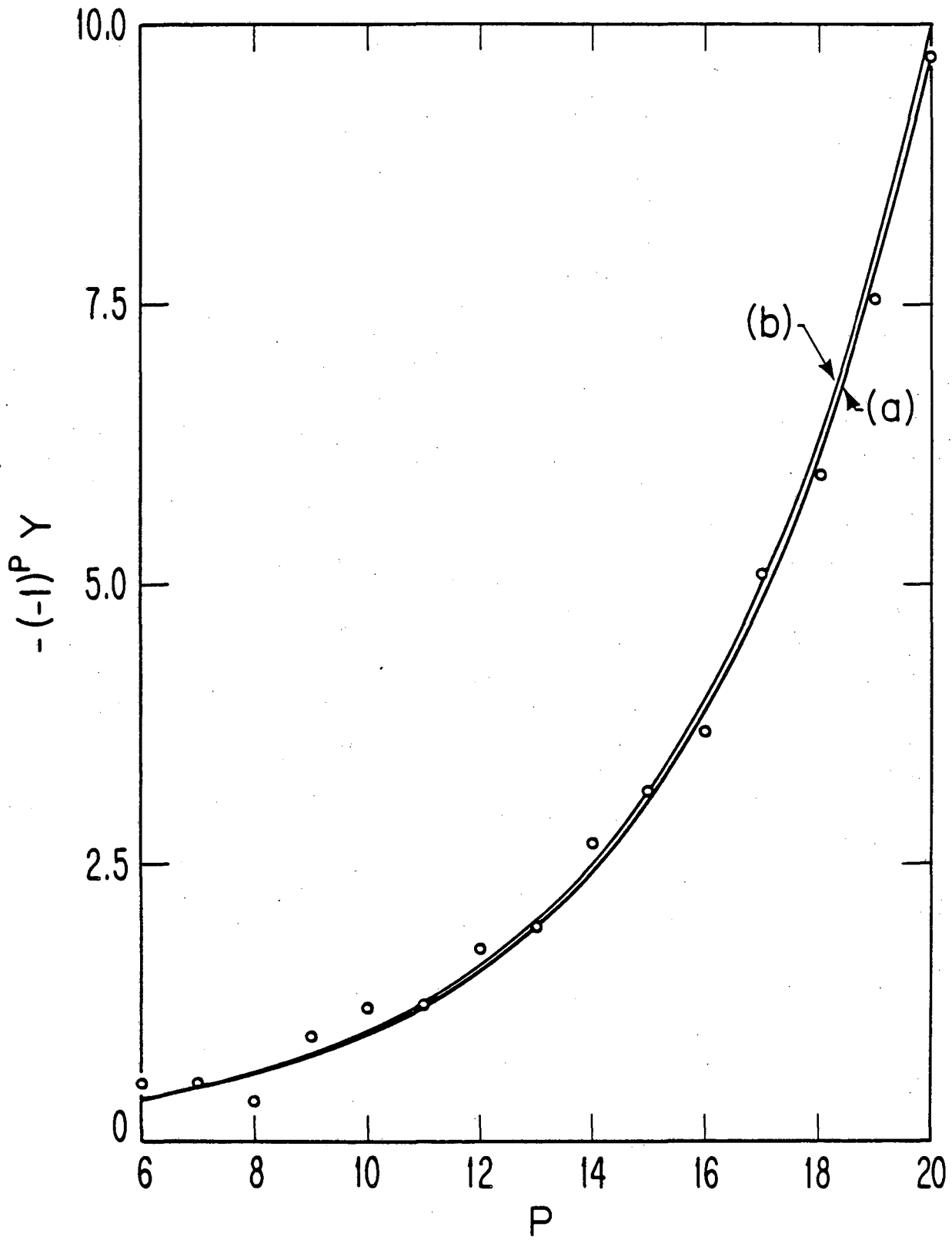
XBL 7910 - 4267

Figure 11



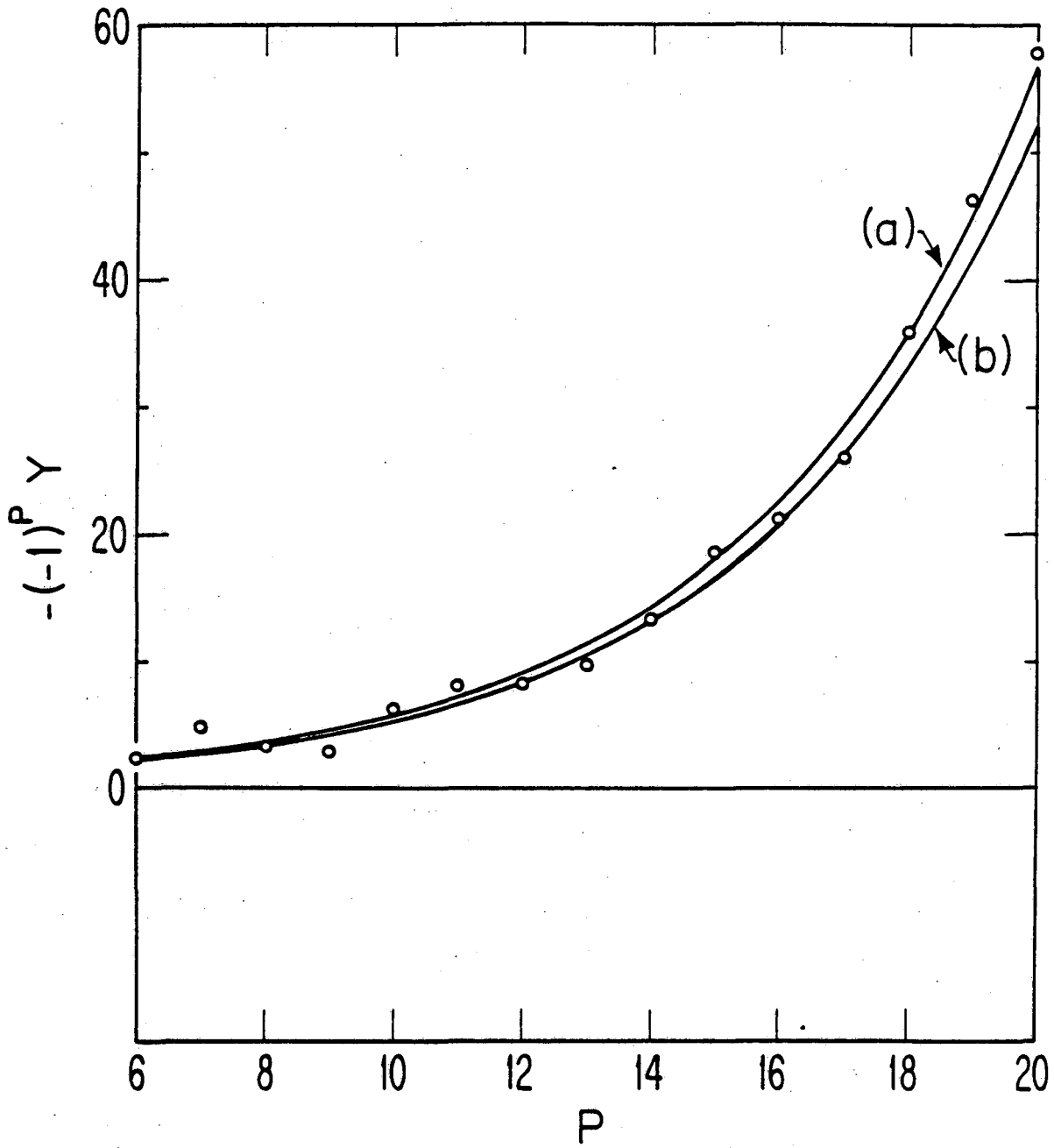
XBL 7910 - 4271

Figure 12



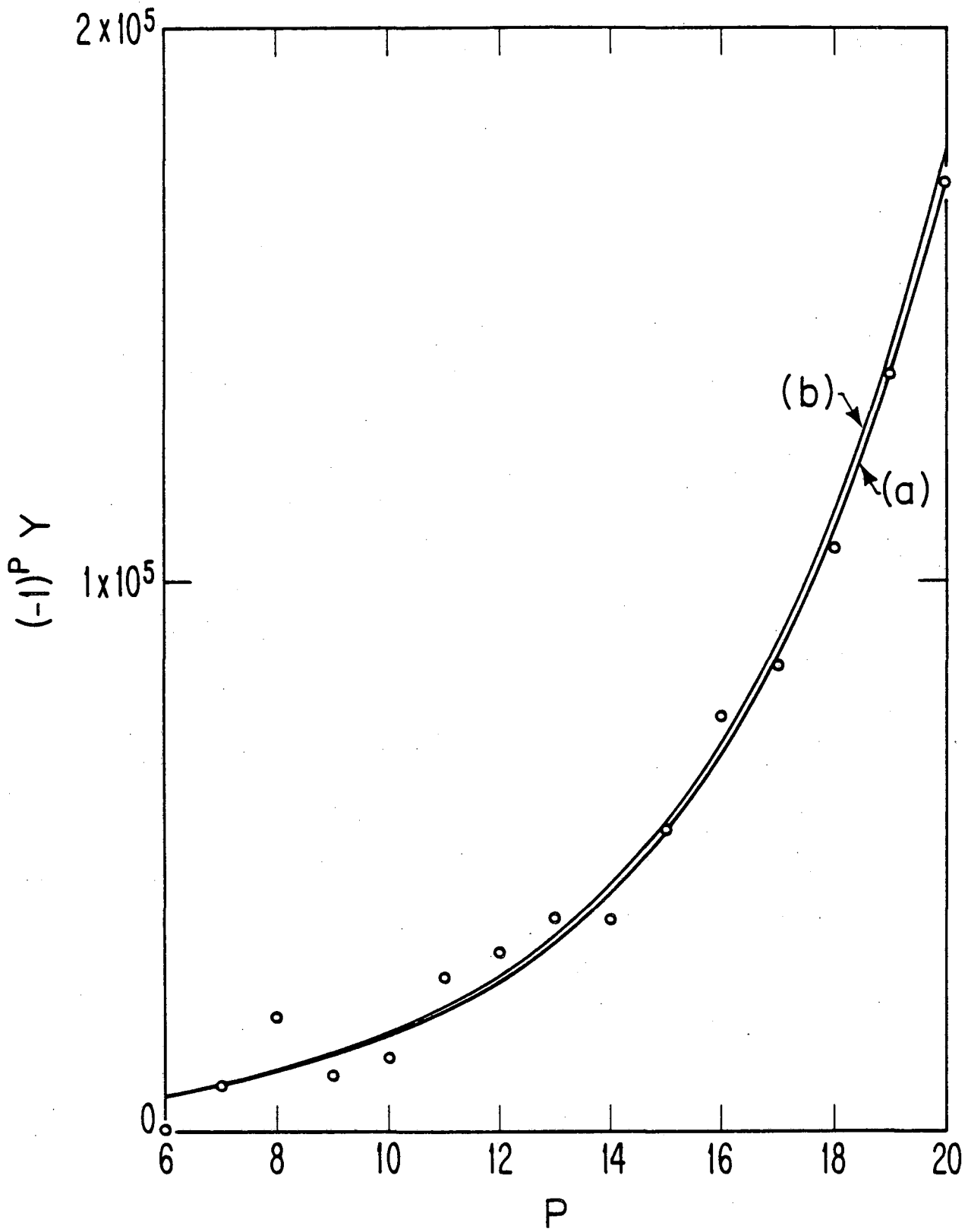
XBL 7910-4275

Figure 13



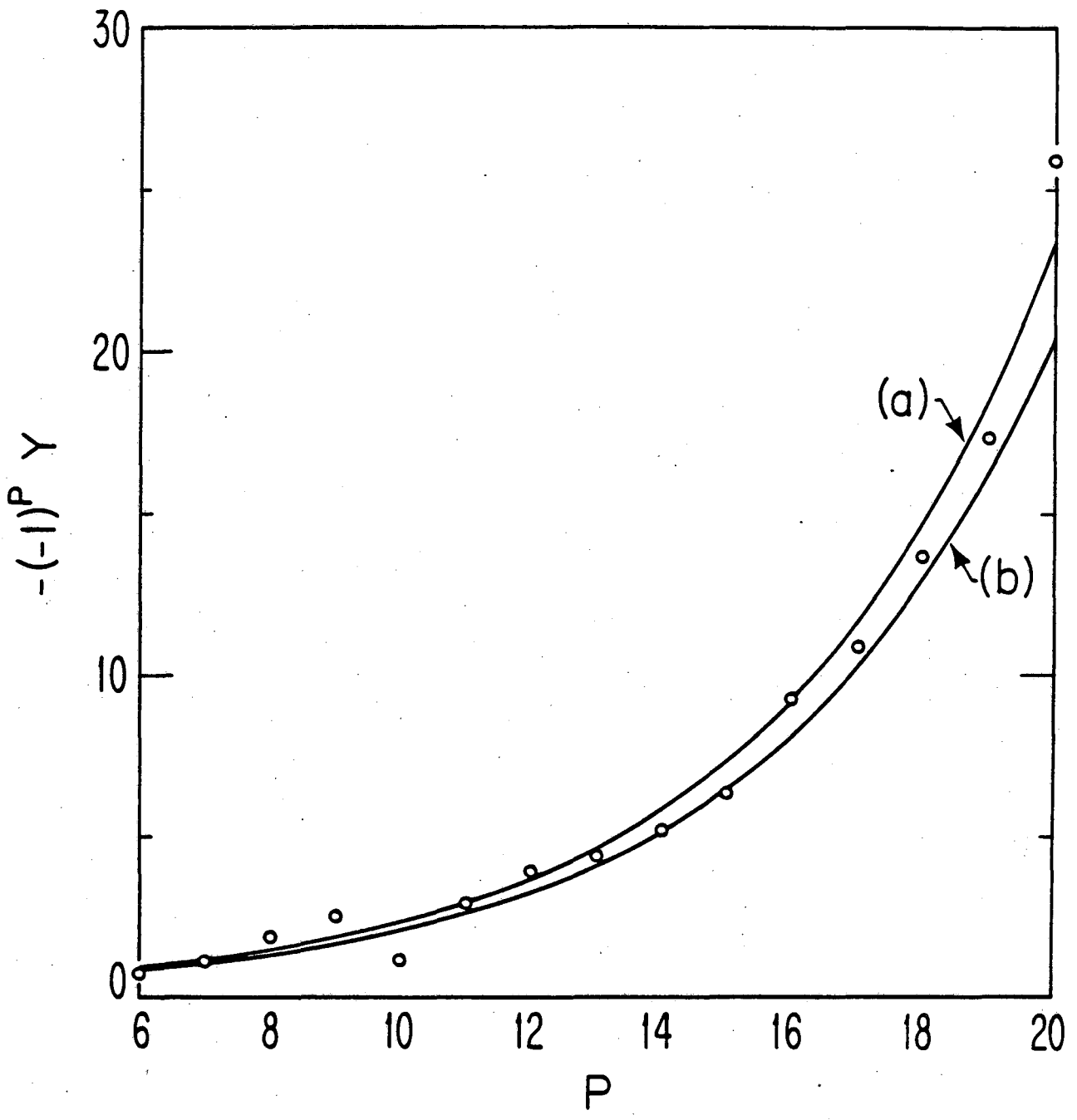
XBL 7910-4274

Figure 14



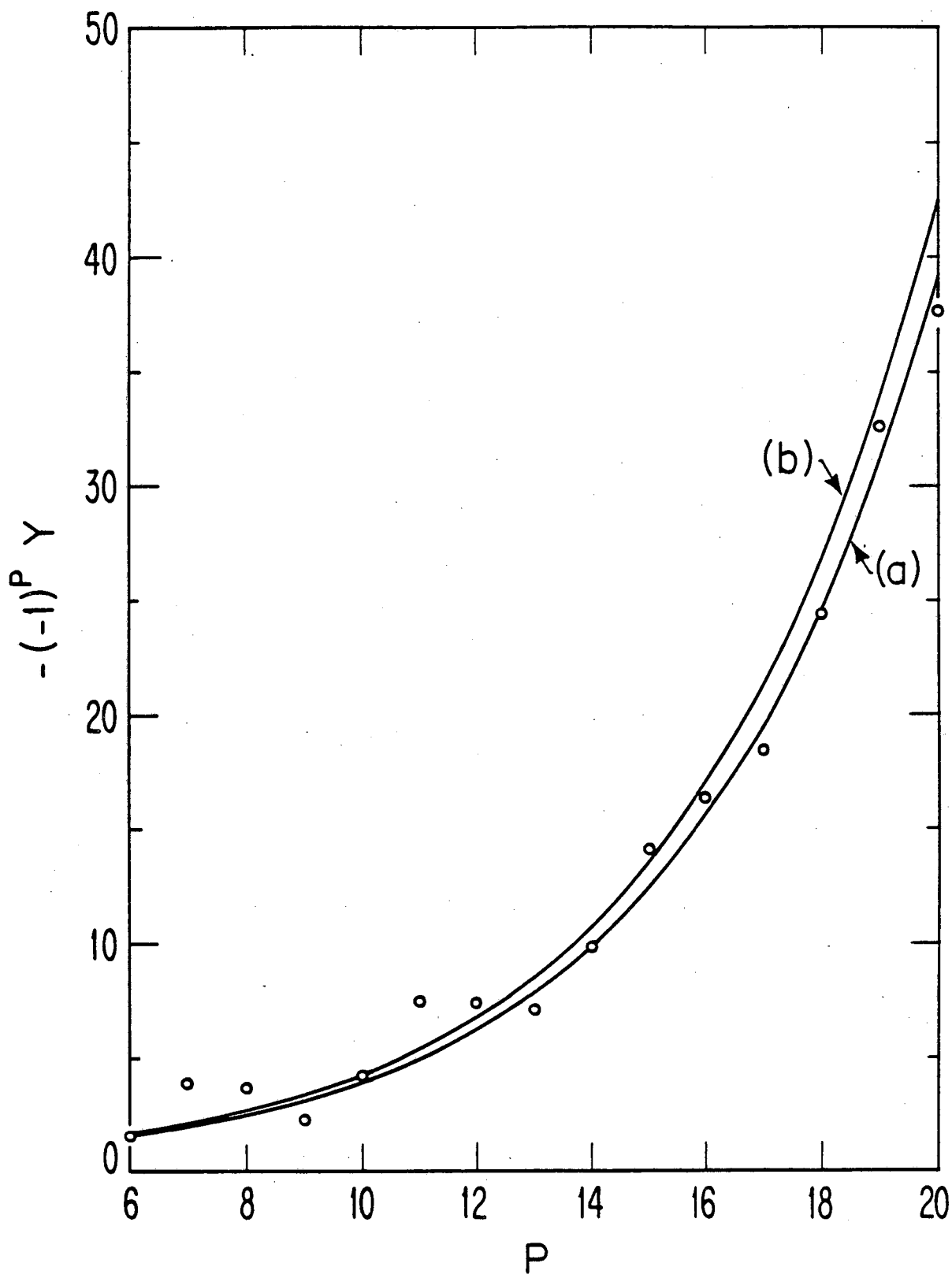
XBL 7910 - 4276

Figure 15



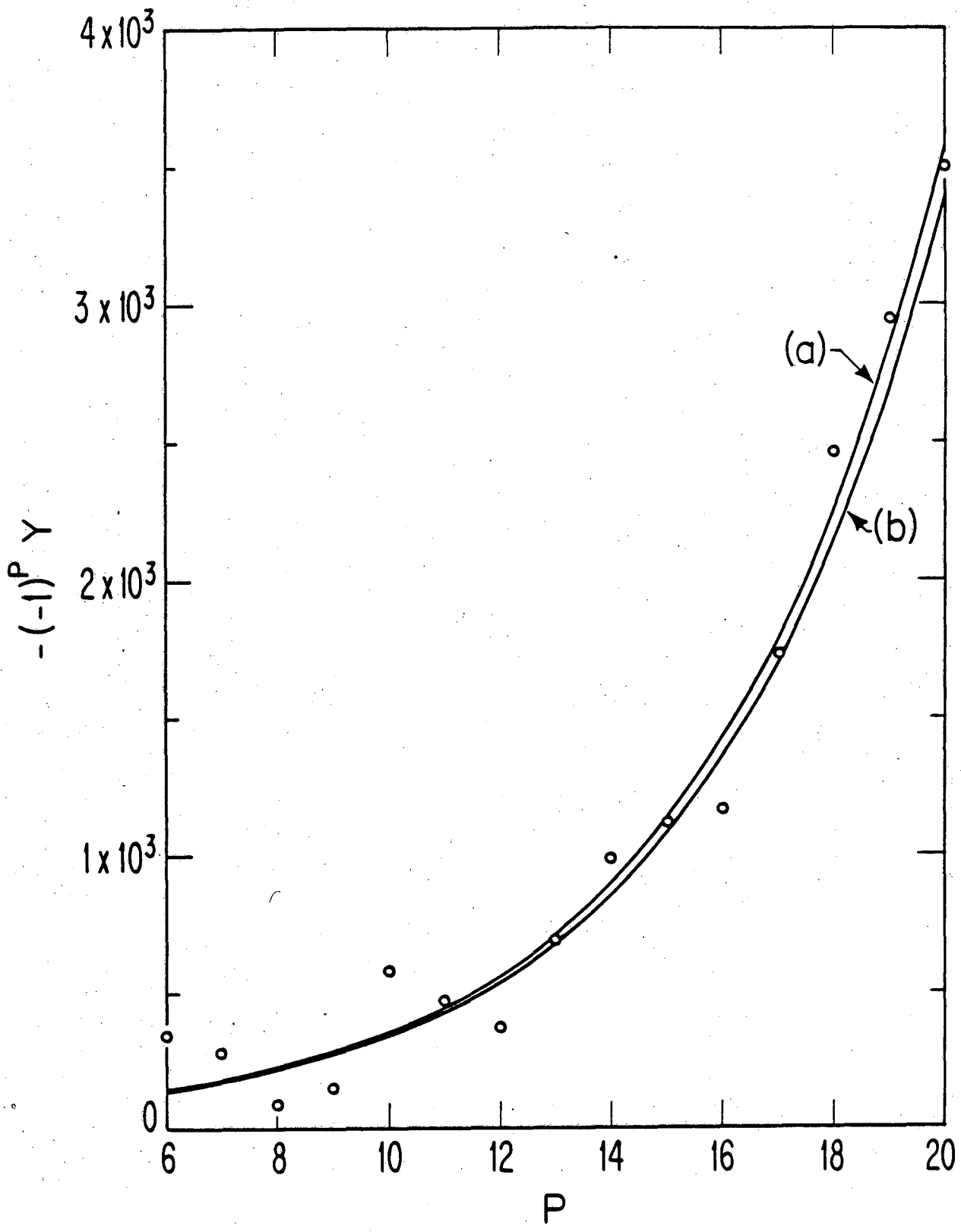
XBL 7910-4277

Figure 16



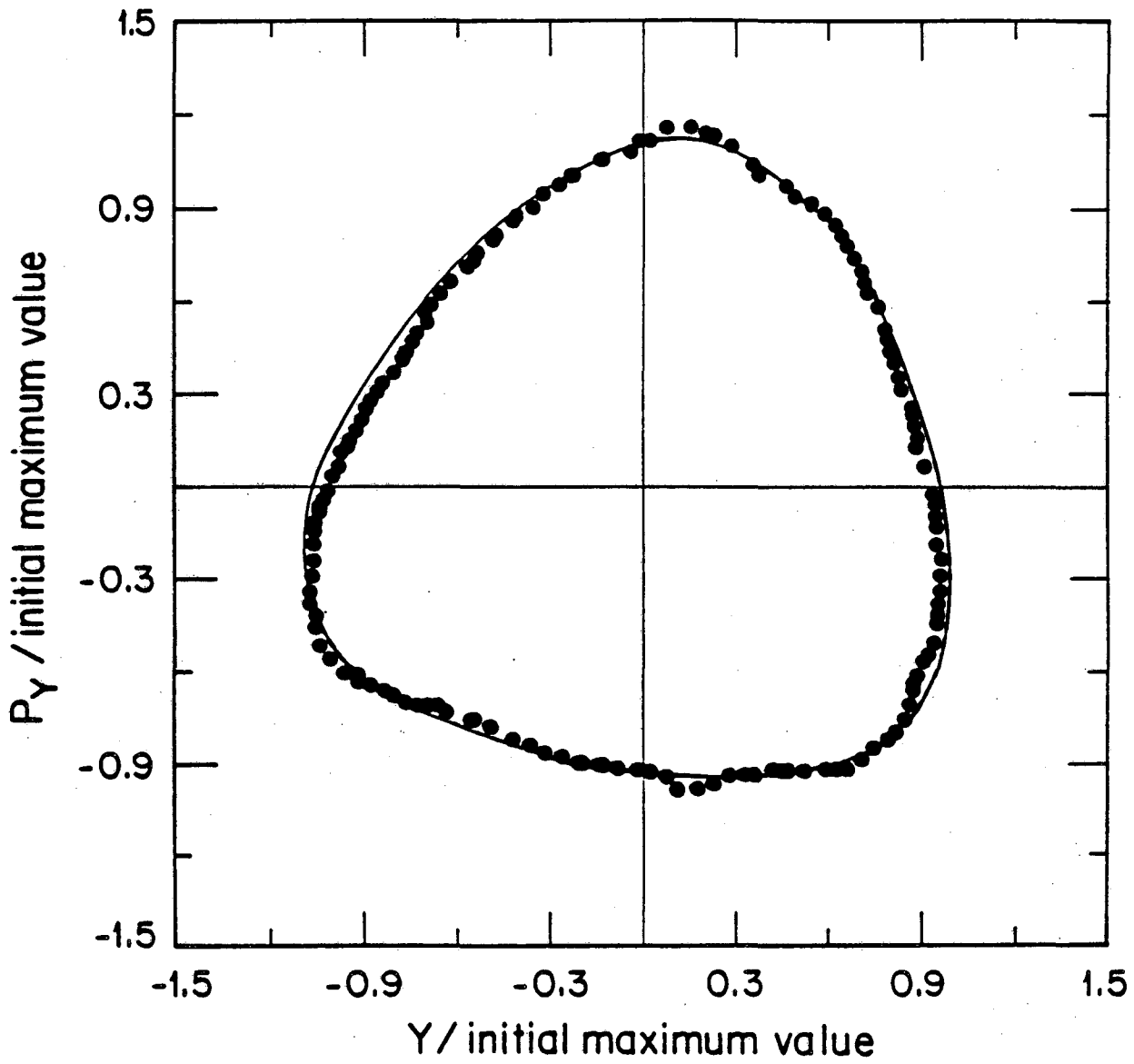
XBL 7910-4273

Figure 17



XBL 7910 - 4272

Figure 18



XBL 7910 - 4269

Figure 19

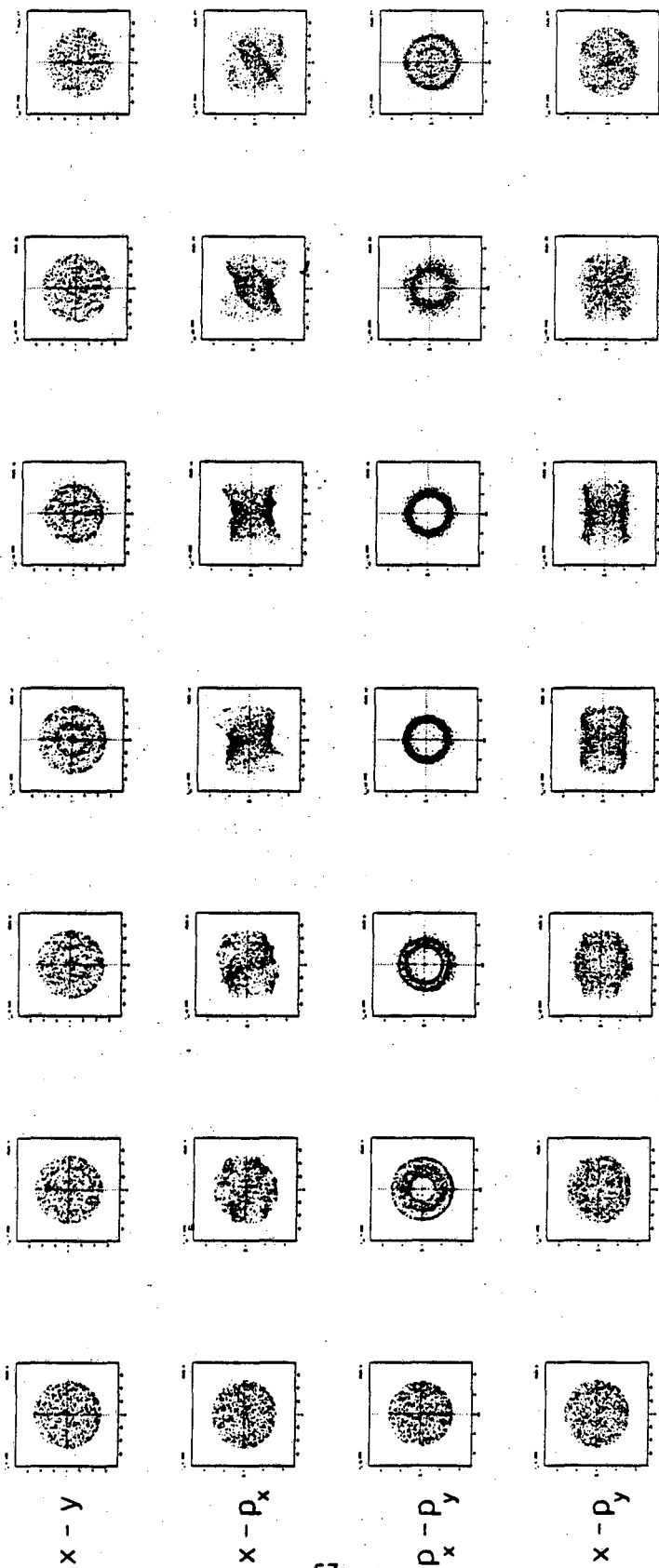
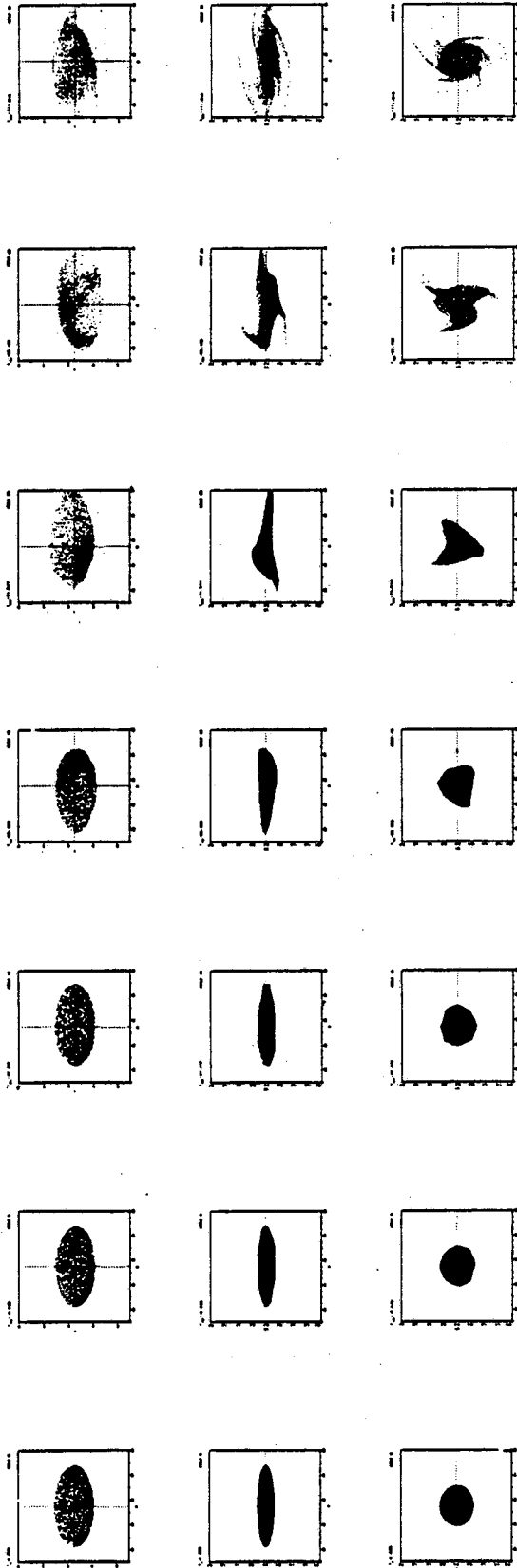


Figure 20



$x - y$

$x - P_x$

$y - P_y$

Figure 21

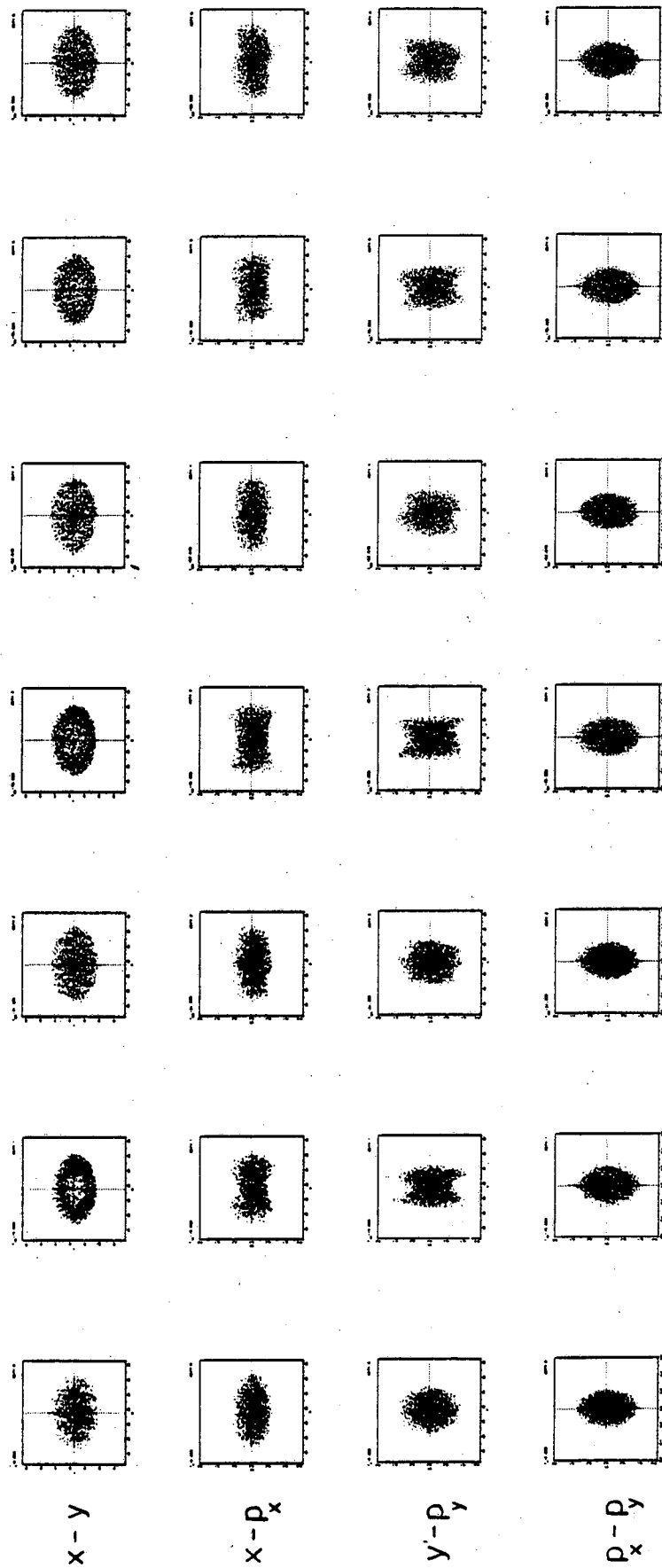


Figure 22

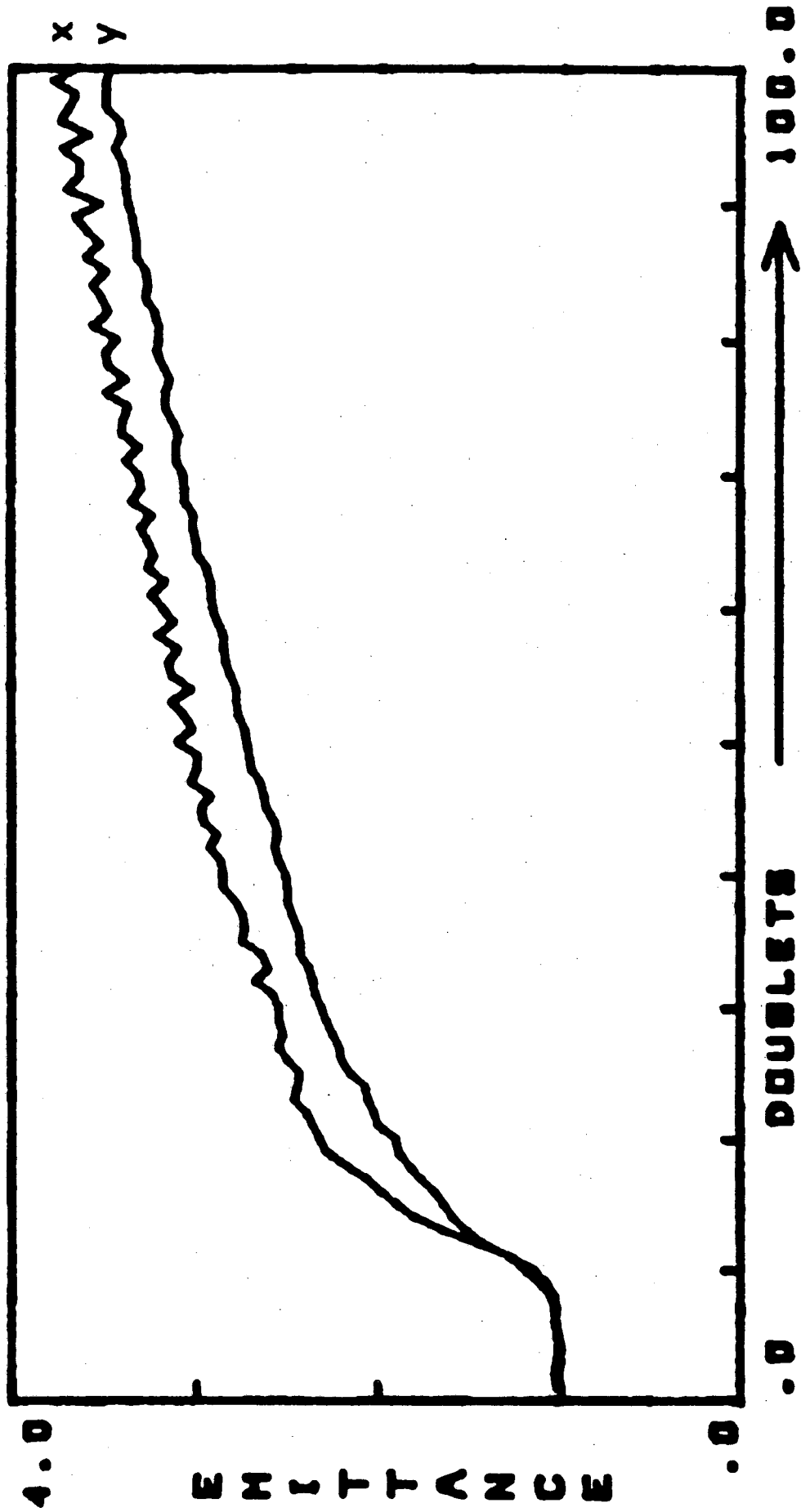


Figure 23

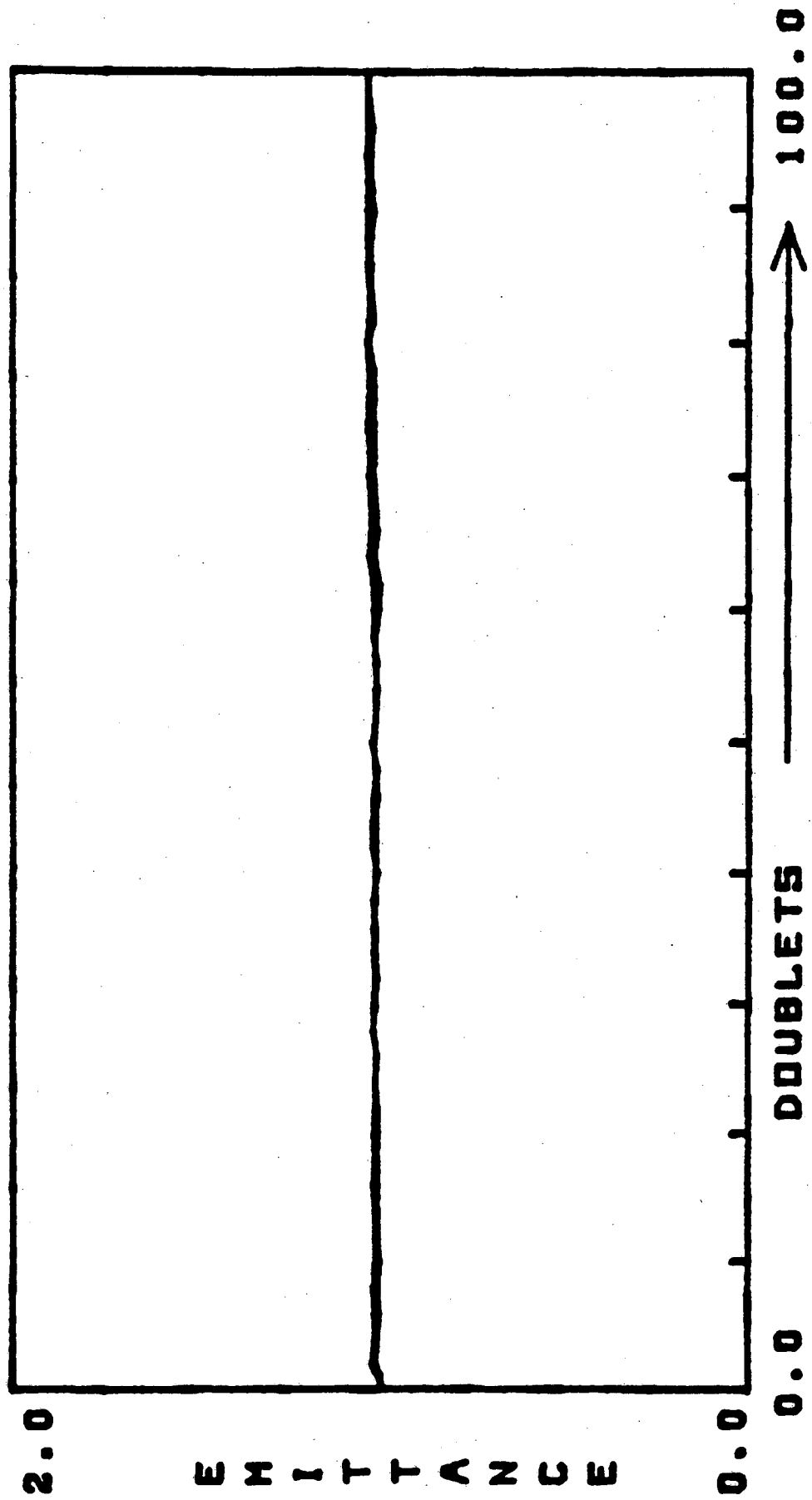


Figure 24

This report was done with support from the Department of Energy. Any conclusions or opinions expressed in this report represent solely those of the author(s) and not necessarily those of The Regents of the University of California, the Lawrence Berkeley Laboratory or the Department of Energy.

Reference to a company or product name does not imply approval or recommendation of the product by the University of California or the U.S. Department of Energy to the exclusion of others that may be suitable.

TECHNICAL INFORMATION DEPARTMENT
LAWRENCE BERKELEY LABORATORY
UNIVERSITY OF CALIFORNIA
BERKELEY, CALIFORNIA 94720